Memoirs of the Faculty of Engineering, Nagoya University
Vol. 31, No. 1. (1979)

NEUTRON DIFFUSION AND THERMALIZATION PARAMETERS: MEASUREMENTS WITH GRAPHITE AND THEORETICAL REVIEW

KOJIRO NISHINA, SHIKOH ITOH, YOSHIHIRO YAMANE, YOSHIO OHMORI and HAJIME TAMAGAWA

Department of Nuclear Engineering

(Received May 30, 1979)

Abstracts

Underlying theories of thermal neutron diffusion length and pulsed-neutron decay constant are introduced. Then follow reports on the measurements of these quantities which were carried out with graphite at Nuclear Engineering Department in 1971. This series of experiments produced nuclear reactor physics parameters (L, $\bar{\Sigma}_a$, $\bar{D}\cdot\bar{v}$ and C) of graphite in reasonable agreement with published values. The discrepancies in some of the parameters are discussed.

After the report, the recent developments in neutron thermalization theory are reviewed. In particular, the minimum transverse size of a graphite prism required in diffusion length measurement is derived following William's work. Then the mechanism of pseudo-discrete mode, which appears as a single exponential decay in pulsed-neutron experiment, is illustrated following Corngold and Durgun's work.

The present article is intended to present an introductory, simple review of the efforts in this field by these two examples. It is intended to make this field accessible to broad range of researchers in both within and outside this field. Possibilities of further investigation on neutron transport are discussed for thermal (0−0.1 ev) and fast (0.1−15 Mev) neutron energy ranges.

CONTENTS

Ⅰ. Introduction

In order to initiate reactor physics experiment program at Nuclear Engineering Department, reactor grade graphite blocks were purchased in 1970. The objective was to learn basic aspects of neutron diffusion and slowing down which are the fundamental elements in neutron balance consideration of nuclear reactors. In the following some of the experimental results are reported. As the order of presentation we first introduce underlying theory in these experiments. Then data on diffusion length measurements and pulse decay experiments are presented with details of experimental set-up. Afterwards some of the recent development in neutron thermalization theory related to these experiments are reviewed and discussed. By such review we intend to speculate possibilities of further investigations in this field, and expose the material in a form accessible to broader groups of researchers.

Because of its low absorption cross section and moderate price, graphite is accepted in general as the most familiar neutron moderator beside ordinary water. It has been extensively used since the days of Manhattan Project during the World War Ⅱ. The additional, specific reasons for the choice of this material in our case are:

(1) It is easily obtainable. Other universities had installed subcritical assemblies, but the procedures in obtaining fissionable material such as uranium appeared burdensome.

(2) The maintenance of moderator is much easier than fissionable material. The material can be accepted in a university campus without special regulation.

(3) Its price was well within the available budget.

In retrospect, it seems to have been a wise choice also from academic reason. The graphite has a mass number of twelve, which makes the various approximations in theory legitimate: Neutron scattering by the material can be assumed to be isotropic in lab system, and Fermi's continuous slowing-down model is acceptable. The temporal variation of neutron density within the material is slow because of little absorption and large slowing-down time. Thus the measurement could be made without much refinement in instrumentation. The material is now serving much educational purpose as well.

In the middle of 1960's, experimental findings in pulsed-neutron decay appeared paradoxical[1] with respect to the then existing theories, which awakened the zeal of theoreticians and experimentalists in this basic field. After frequent international meetings in late 1960's, the findings now seem to have been established and accepted.[2] The structure of the theories possesses a special charm as academic subjects, and an overall review with digestible presentations seems now in order.

To adapt the subjects to rather limited space, the presentations will be confined to two topics, namely neutron diffusion length (Sec. Ⅲ to Sec. Ⅴ), and neutron-pulse decay constant (Sec. Ⅵ to Sec. Ⅷ). Both treatments will be commenced with brief introductions (Sec. Ⅲ and Sec. Ⅵ); the reports of the measurements will then follow (Sec. Ⅳ and Sec. Ⅶ), which were carried out at Nuclear Engineering Department. Finally by further theoretical review on Williams'[3] and Corngold and Durgun's works[4] (Sec. Ⅴ and Sec. Ⅷ), the complex nature of the subjects is pointed out. In particular, we attempt to fill the explanatory gaps of the original papers, which these authors took for granted because of the lack of space.

The details of the theoretical developments overseas during the late 1960's interested only limited number of researchers in this country, in spite of the fact that the conclusions out of the developments were quickly accepted and utilized for data interpretation. Then, hopefully the present review will pave the way to further investigations within this field, and stimulate analogous applications in other fields.

Ⅱ. Three Typical Experiments on Thermal Neutron Diffusion

There are three traditional experiments with which people have determined neutron diffusion- and thermalization parameters. They are spatial-decay measurement, pulse-decay measurement, and so-called neutron-wave experiment, which simply means the experiment with modulated intensity of neutron source. Although all three experiments can be carried out with both multiplying and non-multiplying media, we limit our present discussions to those experiments with the latter. The spatial-decay measurement in such a case is called diffusion-length measurement. In the following (Sec. Ⅱ—1～Ⅱ—3), we introduce these three experiments briefly with formulae derived from one-speed diffusion theory.

Ⅱ—1. *Diffusion Length Measurement*[5],[6]

A rectangular parallelepiped stack of moderating material is constructed, in which a neutron source of constant intensity is placed. The neutrons undergo diffusion, leakage, and absorption, and as a result their density along z-axis attenuates according to the form $e^{-\alpha_0 z}$. The attenuation constant α_0 can be related to diffusion length L as

$$\alpha_0^2=\left(\frac{\pi}{a}\right)^2+\left(\frac{\pi}{b}\right)^2+\frac{1}{L^2} \qquad (\text{Ⅱ}-1)$$

from which one can determine L. The constants a and b denote the transverse (x- and y- direction) dimensions of the stack, with some corrections. The diffusion length L is related to other reactor physics constants by

$$L^2=D/\Sigma_a, \qquad (\text{Ⅱ}-2)$$

where D is diffusion coefficient that appears in Fick's law, and Σ_a is macroscopic absorption cross section. Here and in what follows the constants a and b are made larger than actual dimensions (a_0 and b_0) of the system by an amount $2d=2\times 0.71\,\lambda_{tr}$, so that the formula accounts for the flux distribution near the surface.[7] The quantity λ_{tr} is transport mean free path, and d is called extrapolation distance.

Ⅱ—2. *Pulsed-Neutron Decay Constant*[8],[9]

A neutron source with pulsing function is placed within or adjacent to a parallelepiped system of dimension $a_0(\mathrm{cm})\times b_0(\mathrm{cm})\times c_0(\mathrm{cm})$. The decay of neutron population within the system is observed over a time range of microseconds to milliseconds after the pulse. Due to absorption and leakage, the population undergoes the decay of $e^{-\lambda t}$ form, and reactor physics parameters are related to the constant λ as

$$\lambda=v(\Sigma_a+DB_0^2) \qquad (\text{Ⅱ}-3)$$

by first approximation, where

$$B_0^2=\pi^2\left(\frac{1}{a^2}+\frac{1}{b^2}+\frac{1}{c^2}\right), \qquad c=c_0+2d, \qquad (\text{Ⅱ}-4)$$

and v is neutron speed. The constants Σ_a and D can be determined by curve-fitting on a λ versus B_0^2 curve.

Ⅱ—3. *Neutron-Wave (Modulated Source) Experiment*[10],[11],[12]

Although it bears the name "wave experiment," it does not mean solutions of wave equation, but rather solutions of diffusion equation in response to a source of modulated intensity with angular frequency ω. The neutron source is again placed in contact with a parallelepiped system of Sec. Ⅱ—2, and variation of amplitudes and phases along one co-ordinate axis is observed. The quantities vary according to $\exp\{-(\gamma+i\beta)x+i\omega t\}$, where γ and β can be related to medium parameters as

$$\gamma,\ \beta=\left[\{\sqrt{\alpha_0^4+(\omega/vD)^2}\pm\alpha_0^2\}/2\right]^{1/2} \qquad (\text{Ⅱ}-5)$$

where α_0 is that defined by Eq. (Ⅱ—1), and where the plus sign corresponds to γ, and the minus sign to β. By proper data processing on γ and β, the constants L and D can be determined.

Ⅱ—4. *General Remarks*

The above three experiments had all been initiated before or during 1950's. Then in late 1950's and early 1960's followed more extensive invesigations on neutron thermalization process,[13],[14],[15],[16],[17],[18] which improved the understanding on these experiments greatly. First of all, slight corrections proved necessary on the parameters α, λ, and $(\gamma+i\beta)$, so that the quantities include the deviation of neutron spectrum from equilibrium with moderator. Moreover, a puzzling situation was reported on the determination of λ: theory predicted[18] a certain upper limit on this time eigenvalue of linear transport equation, while experimentalists reported λ values beyond this limit. Such a puzzle was attacked as a subject of mathematical physics by many researchers.[16],[17],[19],[20],[21] It turned out that analogous situations exist on the other two experiments. In Secs. Ⅴ and Ⅷ, we intend to touch upon some of the conclusions[3],[21], taking a glimpse of rich outcome from those activities.

Ⅲ. Theory of Diffusion Length Experiment

We start our discussion with diffusion length L, which is one of the most fundamental quantities that describe neutron diffusion.[22],[5],[23] After theory and measured data are introduced in Secs. Ⅲ and Ⅳ, we will discuss in Sec. Ⅴ the case where this quantity cannot be defined.

Ⅲ—1. *One-speed Theory*

Suppose an infinite plane of neutron source, whose intensity is S_0 neutrons/sec-cm^2, is placed within infinite moderating medium. The plane is assumed to emit source neutrons isotropically with thermal energy, which is an idealized situation. In reality, a source emits fast noutrons, which is moderated and acts as thermal source neutrons distributed over the medium. The resulting thermal neutrons within the moderator obey approximately Maxwellian energy distribution with temperature T_n, which is slightly different from moderator temperature T_m.[24] Much effort has been devoted in predicting the temperature difference $T_n - T_m$.[24]

Although such details should not be overlooked, one can gain a quick insight by assuming that a plane source of thermal neutrons is placed, and that spatial distribution of thermal flux can be described by one-speed diffusion equations with parameters averaged over Maxwellian flux distribution. Therefore

$$\bar{D}\frac{d^2\phi_T(x)}{dx^2}-\bar{\Sigma}_a\phi_T(x)+S_0\delta(x)=0, \qquad (Ⅲ—1)$$

where

$$\phi_T(x)\equiv\int_0^{E_c}\phi(x,\ E)dE, \qquad (Ⅲ—2)$$

$$\overline{D} \equiv \frac{\int_0^{E_c} D(E) M(E, T_n) dE}{\int_0^{E_c} M(E, T_n) dE}, \qquad (\text{Ⅲ}-3)$$

$$\overline{\Sigma}_a \equiv \frac{\int_0^{E_c} \Sigma_a(E) M(E, T_n) dE}{\int_0^{E_c} M(E, T_n) dE}. \qquad (\text{Ⅲ}-4)$$

The quantity $\phi(x, E)$ is energy-dependent neutron flux at energy E (with the unit of neutrons/cm^2-sec-eV), and the interval $(0, E_c)$ defines thermal energy range. The distribution $M(E, T_n)$ is Maxwellian flux distribution, which is energy dependent neutron flux whose density obeys Maxwellian density distribution.[25] A normalized expression of $M(E, T_n)$ is thus

$$M(E, T_n) = \{E/(kT_n)^2\} \cdot \exp\{-E/(kT_n)\}. \qquad (\text{Ⅲ}-5)$$

The solution of Eq. (Ⅲ—1) is given by

$$\phi_T(x) = \frac{LS_0}{2\overline{D}} \exp(-|x|/L), \qquad (\text{Ⅲ}-6)$$

where L is defind as

$$L^2 \equiv \overline{D}/\overline{\Sigma}_a, \qquad (\text{Ⅲ}-7)$$

which is a modified version of the definition (Ⅱ—2). The physical meaning of L^2 is 1/6 times the average of the square of the crow-flight distance from the point where a neutron is introduced to the point where it is absorbed.[22]

Ⅲ—2. *Modified One-speed theory* (1): *Slowing Down Density*

In the above idealized situation, one could determine the value of L by observing the e-fold attenuation of thermal neutron flux within infinite medium. In reality, however, many factors complicate the matter. They are (a) the finiteness of the medium, (b) the energy of source neutrons being different from thermal energy. In the following we will modify the expression (Ⅲ—6) according to Refs. (26) and (6). Our objective is to derive a working formula useful for data processing rather than more-or-less idealized expressions usually found in textbooks.

Suppose there is a rectangular prism of moderator which is infinitely long in z-direction, and measures a cm and b cm along x- and y- directions (including extrapolation distance), respectively (Fig. 1). A point source of fast neutrons whose intensity is S_0 neutrons/sec is placed at the point $P(x_0, y_0, z_0)$, and we seek slowing-down density $q(x, y, z, \tau)$, which is the number of neutrons per second per unit volume crossing energy $E(\tau)$. The quantity τ is called Fermi-age of neutrons and the quantity $q(x, y, z, \tau)$ satisfies an equation

$$\nabla^2 q = \partial q/\partial \tau, \qquad (\text{Ⅲ}-8)$$

if no absorption takes place during moderation. The source intensity distribution $S(x, y, z)$ is expressed by

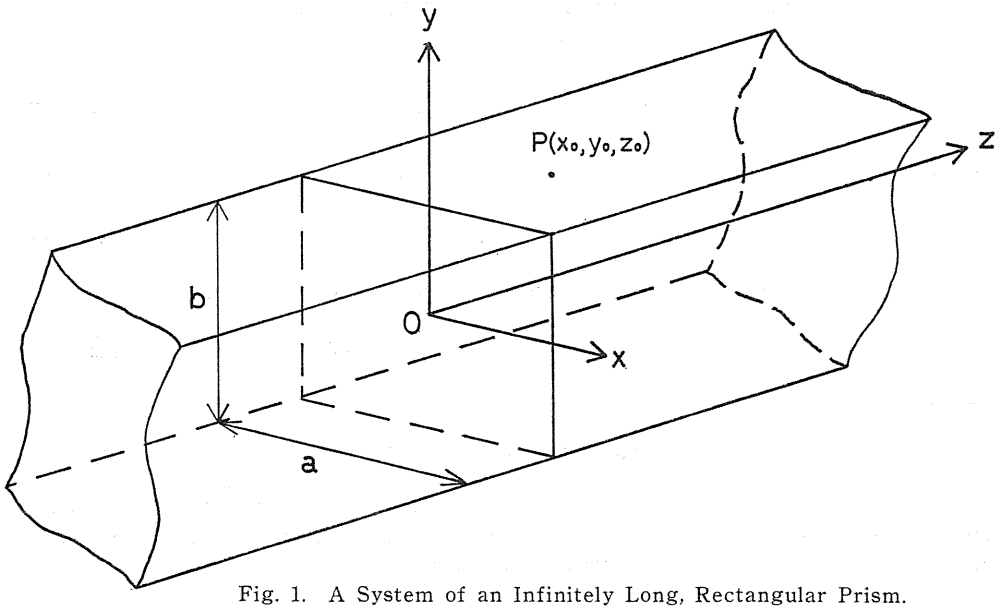

Fig. 1. A System of an Infinitely Long, Rectangular Prism.

$$S(x,\ y,\ z)=S_0\delta(z-z_0)\delta(x-x_0)\delta(y-y_0), \qquad (\text{Ⅲ}-9)$$

which can be set equal to the slowing-down density at $\tau=0$, namely

$$q(x,\ y,\ z,\ 0)=S_0\delta(z-z_0)\delta(x-x_0)\delta(y-y_0). \qquad (\text{Ⅲ}-10)$$

Because we are observing the attenuation in z-direction, we expand the initial ($\tau=0$) distribution (Ⅲ—10) with the eigenfunctions in transverse directions. Thus

$$q(x,\ y,\ z,\ 0)=S_0\delta(z-z_0)\sum_{\substack{1\le k\\ 1\le l}}^{\infty} X_k(x_0)X_k(x)Y_l(y_0)Y_l(y), \qquad (\text{Ⅲ}-11)$$

where

$$X_k(x)=\begin{cases}\sqrt{\dfrac{2}{a}}\cos\dfrac{k\pi x}{a}, & \text{for odd } k,\\ \sqrt{\dfrac{2}{a}}\sin\dfrac{k\pi x}{a}, & \text{for even } k,\end{cases} \qquad (\text{Ⅲ}-12)$$

and

$$Y_l(y)=\begin{cases}\sqrt{\dfrac{2}{b}}\cos\dfrac{l\pi y}{b}, & \text{for odd } l,\\ \sqrt{\dfrac{2}{b}}\sin\dfrac{l\pi y}{b}, & \text{for even } l.\end{cases} \qquad (\text{Ⅲ}-13)$$

The eigenfunctions are so chosen that they can express an asymmetric source position, and that they vanish on the extrapolated boundaries at $x=\pm a/2$, and $y=\pm b/2$. The origin of the co-oridinate is placed at the center of the x-y cross-sectional area.

The solution of Fermi age equation (Ⅲ—8) can be obtained by expanding $q(x, y, z, \tau)$ as

$$q(x, y, z, \tau)=\sum_{k,l} X_k(x)Y_l(y)G_{kl}(z, \tau). \qquad (Ⅲ—14)$$

We define Fourier transform of the coefficient $G_{kl}(z, \tau)$ by

$$\tilde{G}_{kl}(p, \tau)\equiv\int_{-\infty}^{\infty} G_{kl}(z, \tau)e^{-ipz}dz. \qquad (Ⅲ—15)$$

By substitution of Eq. (Ⅲ—14) into age-equation (Ⅲ—8), we obtain

$$\tilde{G}_{kl}(p, \tau)=C_{kl}(p)\exp\{-(p^2+B_{kl}^2)\tau\}, \qquad (Ⅲ—16)$$

where

$$B_{kl}^2=(k\pi/a)^2+(l\pi/b)^2, \qquad (Ⅲ—17)$$

and where $C_{kl}(p)$ is a function of p only which can be determined by imposing the Fourier transform of the condition (Ⅲ—11) upon $\tilde{G}_{kl}(p, \tau)$. By inversion of $\tilde{q}(x, y, p, \tau)$, the slowing-down density is found to be[27]

$$q_\infty(x, y, z, \tau)=S_0(4\pi\tau)^{-1/2}\exp\{-(z-z_0)^2/4\tau\}\cdot$$
$$\cdot\sum_{k,l} X_k(x_0)X_k(x)Y_l(y_0)Y_l(y)\exp(-B_{kl}^2\tau), \qquad (Ⅲ—18)$$

where a subscript ∞ is attached to indicate the solution for an infinitely long prism.

If the prism is finite in z-direction with a dimension of c (cm), the solution of the age-equation (Ⅲ—8) takes the form

$$q_{fin}(x, y, z, \tau)=S_0\sum_{k,l,m=1}^{\infty}\exp(-B^2{}_{klm}\tau)X_k(x_0)X_k(x)\cdot$$
$$\cdot Y_l(y_0)Y_l(y)Z_m(z_0)Z_m(z), \qquad (Ⅲ—19)$$

where

$$Z_m(z)=\begin{cases}\sqrt{\dfrac{2}{c}}\cos\dfrac{m\pi z}{c} & \text{for odd m,}\\ \sqrt{\dfrac{2}{c}}\sin\dfrac{m\pi z}{c} & \text{for even m.}\end{cases} \qquad (Ⅲ—20)$$

and where

$$B_{klm}^2=\pi^2\{(k/a)^2+(l/b)^2+(m/c)^2\}. \qquad (Ⅲ—21)$$

The subscript "*fin*" on q indicates the solution for a finite system.

Because the present experiments are carried out in a finite system, it may appear that the solution q_{fin} of (Ⅲ—19) is more appropriate for our data analysis than q_∞ in (Ⅲ—18). If one is to use q_{fin} for this reason, the procedure would be as follows: Let τ_{th} denote the age of neutrons at E_c (the upper limit of thermal energy). Then q_{fin} (x, y, z, τ_{th}) would give distributed thermal neutron source originating from slowing-down process. This quantity would be multiplied by

Green's function for thermal neutron flux given later in Sec. Ⅲ—3, and the product would be integrated over the distribution of $q_{fin}(x, y, z, \tau_{th})$. The resulting expression would give position-dependent thermal flux. Such a solution, however, is not suitable for our data processing, because the eigenfunction expansion with $Z_m(z)$ is not fitted for parameter (L) extraction out of z-dependent detector responses.

It is better to construct a solution from q_∞, which vanishes at the boundary $z=\pm c/2$. (The origin is placed at the center of a parallelepiped). Specifically, we place images of the real source along z-direction, and take a superposition of the q_∞'s originating from these images. The positions of first several images are

$$\begin{aligned} &z=-c-z_0, \quad c-z_0 \qquad \text{for negative images,} \\ &z=-2c+z_0, \quad 2c+z_0 \qquad \text{for positive images.} \end{aligned} \tag{Ⅲ—22}$$

These positions can be determined by inspection, but they can also be determined mathematically by applying Poisson's transformation[28]

$$\sum_{m=-\infty}^{\infty}\varphi(m)=\sum_{k=-\infty}^{\infty}\int_{-\infty}^{\infty}\varphi(\omega)e^{-2\pi ik\omega}d\omega \tag{Ⅲ—23}$$

to q_{fin} of (Ⅲ—19), where m and k are integers.

The resulting approximate expression $q_{app}(x, y, z, \tau)$ after the transformation is

$$q_{app}(x, y, z, \tau)=f(z)\cdot\sum_{k,l}S^0_{kl}X_k(x)Y_l(y) \tag{Ⅲ—24}$$

where

$$S^0_{kl}\equiv\frac{S_0}{\sqrt{4\pi\tau}}e^{-B^2_{kl}\tau}X_k(x_0)Y_l(y_0), \tag{Ⅲ—25}$$

$$f(z)\equiv f_1(z)+f_2(z)+f_3(z), \tag{Ⅲ—26}$$

$$\left.\begin{aligned} f_1(z)&=\exp\{-(z-z_0)^2/4\tau\}, \\ f_2(z)&=-\exp\{-[z+c+z_0]^2/4\tau\}, \\ f_3(z)&=-\exp\{-[z-(c-z_0)]^2/4\tau\}. \end{aligned}\right\} \tag{Ⅲ—27}$$

The solution q_{app} of (Ⅲ—24) is approximate in the sense that it includes only two first negative sources, one at $-(c+z_0)$ and another at $(c-z_0)$, each corresponding to $f_2(z)$ and $f_3(z)$, respectively. The number of images that have to be included in such an approximate solution is dependent on the positions of source and detector in general. In later analysis, the terms $f_1(z)$ and $f_2(z)$ will be sufficient, due to the source position close to the boundary $z=-c/2$.

Ⅲ—3. *Modified One-speed Theory (2): (k, l) Mode Green's Function*

In order to construct thermal neutron flux solution, we need Green's function, which is to be multiplied by q_{app} of (Ⅲ—24) and integrated. Suppose a plane thermal neutron source of (k, l) mode is placed at $z=z_1$ in a form

$$S_{kl}(x, y, z)=S^0_{kl}X_k(x)Y_l(y)\delta(z-z_1), \tag{Ⅲ—28}$$

where the constant S^0_{kl} is given by (Ⅲ—25) with the unit of neutrons/cm²-sec. We seek the solution of diffusion equation

$$\bar{D}\nabla^2 g_{kl}(x,\ y,\ z|z_1)-\bar{\Sigma}_a g_{kl}+S_{kl}(x,\ y,\ z)=0, \qquad (Ⅲ—29)$$

where the function $g_{kl}(x,\ y,\ z|z_1)$ is to be determined under a boundary condition

$$g_{kl}(x,\ y,\ \pm c/2|z_1)=0. \qquad (Ⅲ—30)$$

The solution is given as[29]

$$g_{kl}(x,\ y,\ z|z_1)=\begin{cases} g^{\mathrm{I}}_{kl}(z|z_1)=H_{kl}(x,\ y)\sinh\alpha_{kl}(c/2+z_1)\sinh\alpha_{kl}(c/2-z) \\ \qquad\qquad \text{for } z_1<z, \\ g^{\mathrm{II}}_{kl}(z|z_1)=H_{kl}(x,\ y)\sinh\alpha_{kl}(c/2+z)\sinh\alpha_{kl}(c/2-z_1) \\ \qquad\qquad \text{for } z_1>z, \end{cases} \qquad (Ⅲ—31)$$

where

$$H_{kl}(x,y)=\frac{S^0_{kl}X_k(x)Y_l(y)}{\bar{D}\alpha_{kl}\sinh\alpha_{kl}c}, \qquad (Ⅲ—32)$$

$$\alpha^2_{kl}=1/L^2+B^2_{kl}. \qquad (Ⅲ—33)$$

Note a relation $\alpha_{11}=[\alpha_0$ in Eq. (Ⅱ—1)$]$. For brevity we dropped the variable x and y from the arguments of g^{I}_{kl} and g^{II}_{kl}.

Ⅲ—4. *Modified One-speed Theory* (3): *Formulation of thermal flux*

In actual experiments a fast neutron source of Am—Be or Ra—Be is placed within a stack of moderator (graphite, beryllium or water) and the attenuation of thermal neutron flux along z-axis is observed. In order to secure a long region of single exponential attenuation the source is usually placed near one end of the system.

Suppose we place the source μ_1 cm apart from one end of the system, and shift the origin of z axis to this source position for ease of the following analyses. The source position is then given as $(x_0,\ y_0,\ 0)$ (Fig. 2). The two ends of the stack (including extrapolation distance) are denoted as $z=-\mu_1$ and $z=\mu_2$, respectively ($c=\mu_1+\mu_2$).

With this new system, our $f_1(z)$, $f_2(z)$ and $f_3(z)$ used for q_{app} of (Ⅲ—24) become as follows:

$$\begin{aligned} f_1(z)&=\exp\{-z^2/4\tau\}, \\ f_2(z)&=-\exp\{-(z+2\mu_1)^2/4\tau\}, \\ f_3(z)&=-\exp\{-(z-2\mu_2)^2/4\tau\}. \end{aligned} \qquad (Ⅲ—34)$$

The Green's functions of (Ⅲ—31) are rewritten as

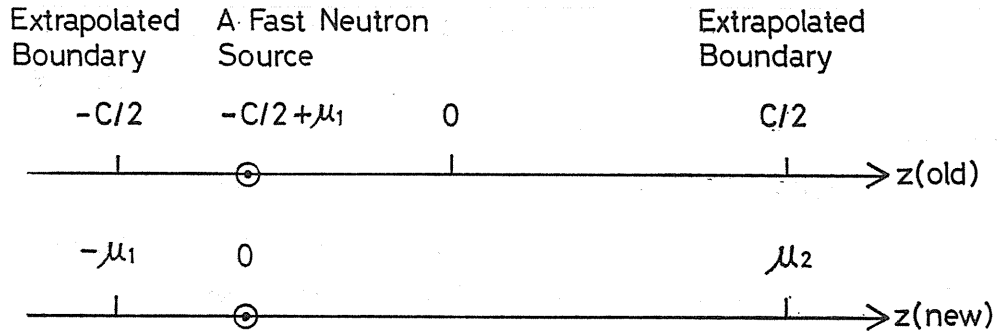

Fig. 2. The Source Position and Co-oridinate System ($c=\mu_1+\mu_2$).

$$g_{kl}(x,\ y,\ z|z_1)=\begin{cases} g^{\mathrm{I}}_{kl}(z|z_1)=H_{kl}(x,\ y)\sinh\alpha_{kl}(\mu_1+z_1)\sinh\alpha_{kl}(\mu_2-z), \\ \qquad\qquad \text{for } z_1<z, \\ g^{\mathrm{II}}_{kl}(z|z_1)=H_{kl}(x,\ y)\sinh\alpha_{kl}(\mu_1+z)\sinh\alpha_{kl}(\mu_2-z_1), \\ \qquad\qquad \text{for } z_1>z. \end{cases} \tag{Ⅲ—35}$$

Then the $(k,\ l)$ mode of the approximate thermal flux is given as

$$\phi^{kl}_{app}(x,\ y,\ z)=\int_{-\mu_1}^{z} g^{\mathrm{I}}_{kl}(z|z_1)f(z_1)dz_1+\int_{z}^{\mu_2} g^{\mathrm{II}}_{kl}(z|z_1)f(z_1)dz_1 \tag{Ⅲ—36}$$

with $\tau=\tau_{th}$ in $f(z_1)$. As further approximation, we disregard $f_3(z_1)$ in $f(z_1)$, and put

$$f(z_1)\approx f_1(z_1)+f_2(z_1),$$

which is reasonable for the present experiment where $\mu_1=56.8$ cm and $\mu_2=146.8$ cm.

The integral in the first term of (Ⅲ—36) can be evaluated as follows: The function

$$J^{\mathrm{I}}_{kl}(z)\equiv\int_{-\mu_1}^{z}\sinh\alpha_{kl}(\mu_1+z_1)\{f_1(z_1)+f_2(z_1)\}dz_1 \tag{Ⅲ—37}$$

in this term can be written as

$$J^{\mathrm{I}}_{kl}(z)=I^{\mathrm{I}}_{kl}(z,\ 0)-I^{\mathrm{I}}_{kl}(z,\ 2\mu_1).$$

The function $I^{\mathrm{I}}_{kl}(z,\ h)$ is defined as follows:

$$I^{\mathrm{I}}_{kl}(z,\ h)\equiv\int_{-\mu_1}^{z}\sinh\alpha_{kl}(\mu_1+z_1)\cdot\exp\{-(z_1+h)^2/4\tau_{th}\}dz_1. \tag{Ⅲ—38}$$

Furthermore, in terms of a function defined by

$$K_{kl}(\eta,\ \alpha_{kl},\ z)\equiv(\sqrt{\pi\tau_{th}}/2)\exp(\alpha_{kl}^2\tau_{th})\exp[\alpha_{kl}(\eta-h)]\times$$
$$\times\mathrm{erf}[(h-2\tau_{th}\alpha_{kl}+z)/2\sqrt{\tau_{th}}], \qquad (\text{Ⅲ}-39)$$

the function $I_{kl}^{\text{I}}\ (z,\ h)$ can be given as

$$I_{kl}^{\text{I}}(z,\ h)=[K_{kl}(\mu_1,\ \alpha_{kl},\ z)-K_{kl}(\mu_1,\ \alpha_{kl},\ -\mu_1)]-$$
$$-[K_{kl}(\mu_1,\ -\alpha_{kl},\ z)-K_{kl}(\mu_1,\ -\alpha_{kl},\ -\mu_1)]. \qquad (\text{Ⅲ}-40)$$

In the second integral of (Ⅲ—36) the following integral appears:

$$J_{kl}^{\text{I}}(z)\equiv\int_z^{\mu_2}\sinh\alpha_{kl}(\mu_2-z_1)\{f_1(z_1)+f_2(z_1)\}dz_1$$
$$=I_{kl}^{\text{I}}(z,\ 0)-I_{kl}^{\text{I}}(z,\ 2\mu_1), \qquad (\text{Ⅲ}-41)$$

where

$$I_{kl}^{\text{I}}(z,\ h)\equiv[K_{kl}(-\mu_2,\ \alpha_{kl},\ z)-K_{kl}(-\mu_2,\ \alpha_{kl},\ \mu_2)]-$$
$$-[K_{kl}(-\mu_2-\alpha_{kl},\ z)-K_{kl}(-\mu_2,\ -\alpha_{kl},\ \mu_2)]. \qquad (\text{Ⅲ}-42)$$

Using these results we can express the approximate total thermal flux as

$$\phi_{app}(x,\ y,\ z)=\sum_{k,l}\phi_{app}^{kl}(x,\ y,\ z), \qquad (\text{Ⅲ}-43)$$

where

$$\phi_{app}^{kl}(x,\ y,\ z)=H_{kl}(x,\ y)[\sinh\alpha_{kl}(\mu_2-z)\{I_{kl}^{\text{I}}(z,\ 0)-I_{kl}^{\text{I}}(z,\ 2\mu_1)\}$$
$$+\sinh\alpha_{kl}(\mu_1+z)\{I_{kl}^{\text{I}}(z,\ 0)-I_{kl}^{\text{I}}(z,\ 2\mu_1)\}]. \qquad (\text{Ⅲ}-44)$$

The expressions in (Ⅲ—43) and (Ⅲ—44) are approximate in that approximate slowing-down density with only one image source was used in the derivation. We need to know rough estimate of each parameter, in order to further reduce Eq. (Ⅲ—44) to a convenient form. Therefore, further reduction will be made in the next section where a diffusion length experiment is reported.

At this stage, however, we point out that the formula (Ⅲ—44) is quite effective. Usually the attenuation of the $\phi_T\ (x,\ y,\ z)$ along z axis stays far off from a straight line in $\log\phi_T-z$ plot. The correction based on (Ⅲ—44) improves this situation considerably. The improvement is more remarkable for smaller stacks. Furthermore, Eq. (Ⅲ—44) relies on less approximation than are available in literatures.[6] Because we have presented the derivations in more general way, the degree of accuracy can easily be improved, if necessary, by taking higher order terms.

One important consideration for thermal diffusion length measurement is that one cannot determine this quantity with a fast neutron source of high energy, for which the medium has a larger value of τ_{th} than L. Thus one has to devise a neutron source with energy less than 0.1 Mev for measurements in light water.[30]

Ⅳ. Diffusion Length Measurement at Nuclear Engineering Department[26]

Ⅳ—1. *Graphite Block Specifications*

Reactor grade graphite blocks with total volume of 4.8 m^3 were purchased by Nuclear Engineering Department from Showa Denko in March, 1970. "Reactor Grade" implies very little impurity contained. The specifications of these blocks will be given in the following.

There are eleven kinds of rectangular blocks with different dimensions, which are coded as A through K. The major portion of the above total volume is occupied by the blocks of types A ($100\times100\times1,000$ mm^3) and B ($100\times100\times500$ mm^3), which totaled 2.6 m^3 and 1.3 m^3, respectively. Among other kinds, the types I, J, K had longitudinal holes of 65, 42 and 28 mm diameters, respectively, which are used for detector insertion. In the absence of a detector, the holes are filled with cylindrical graphite plugs. In the following diffusion length experiment, a parallelepiped stack of 150 cm×150 cm×200 cm was constructed mainly with the blocks of types A and B, and with ten blocks of type J. Every block was requested to have error less than ±0.07 mm in length, and less than ±0.02 mm in transverse size. The requirements were reported to have been satisfied.[31]

As to impurity, ash content was reported to be 16.4 ppm, and boron content, 0.04 ppm.[31] The following experiment, however, seems to suggest more boron content. Densities of all blocks were requested to be higher than 1.70, and their specific values were submitted in a table.[31] The averages and standard deviations were calculated from the table, and given in Table 1. As a Type A block has twice as much volume as a block of Type B, the values of $\bar{\rho}_A$ and $\bar{\rho}_B$ in the table refer to samples of 1×10^4 cm^3 and 0.5×10^4 cm^3, respectively, being chosen randomly within own types. The values under the entry "A+B" were calculated according to the formula

$$\bar{\rho}_{AB}=(2\bar{\rho}_A+\bar{\rho}_B)/3, \qquad (\text{Ⅳ}-1)$$

$$\sigma^2_{AB}=\{6\sigma^2_A+3\sigma^2_B+2(\bar{\rho}_A-\bar{\rho}_B)^2)\}/9. \qquad (\text{Ⅳ}-2)$$

These quantities concern a sample volume of 0.5×10^4 cm^3 chosen randomly within a stack, which is constructed from 260 blocks of Type A and 260 blocks of Type B.

Table Ⅰ. Densities of Graphite Blocks Used.

Block type	Average density of 260 blocks (g/cm^3)	Standard deviation of 260 blocks (g/cm^3)
A	$\bar{\rho}_A=1.755$	$\sigma_A=0.018$
B	$\bar{\rho}_B=1.757$	$\sigma_B=0.019$
A+B	$\bar{\rho}_{A+B}=1.756$	$\sigma_{A+B}=0.019$

Ⅳ—2. *Detector and Counting System*

A boron-trifluoride (BF_3) proportional counter, which was manufactured by 20th Century Electronics Ltd., Britain, was used as a thermal-neutron detector.

Its type was 12EB40,[32] whose glass capsule was contained in a cylindrical copper of 2.5 cm O.D., and 27.0 cm length. The active length was 12 cm, where BF_3 gas of the pressure 40 cm Hg is filled. The enrichment of ^{10}B is 90% or greater. The sensitivity, defined by (n, α) reaction rate per unit neutron flux, has a unit of {counts/sec}/{neutrons/cm^2·sec}, and is calculated to be 2.84 if enrichment of 100%, and the (n, α) reaction cross section of 3840 barns[33] (for neutrons of 2,200 m/sec) are assumed for ^{10}B. The catalogue[32] gives sensitivity of 3.0 as a measured value. The above specification is important in evaluating perturbation effect of the detector

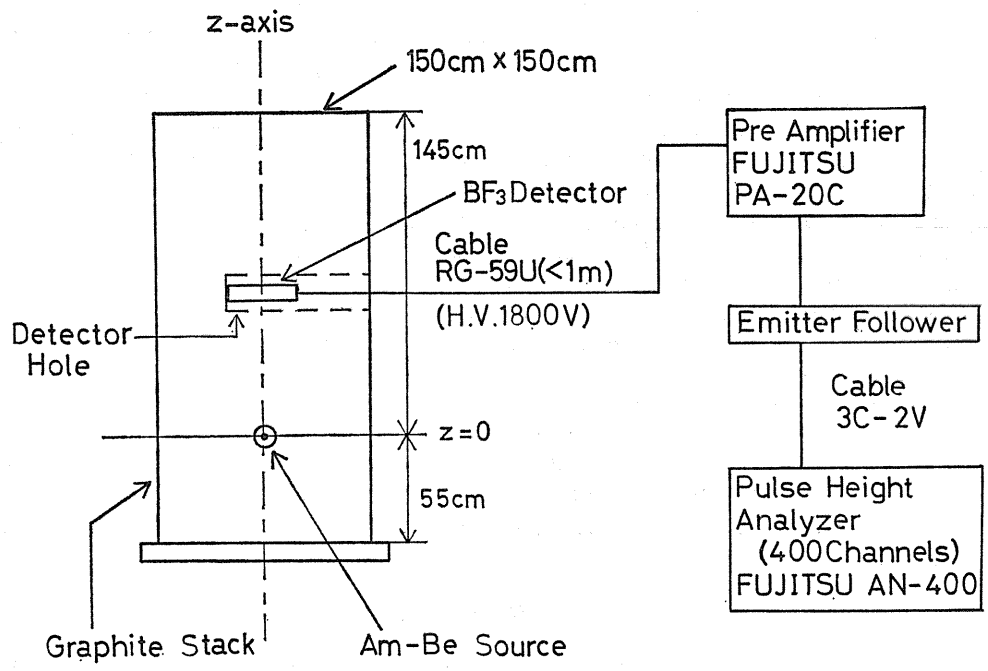

Fig. 3. The Block Diagram of the Counting System.

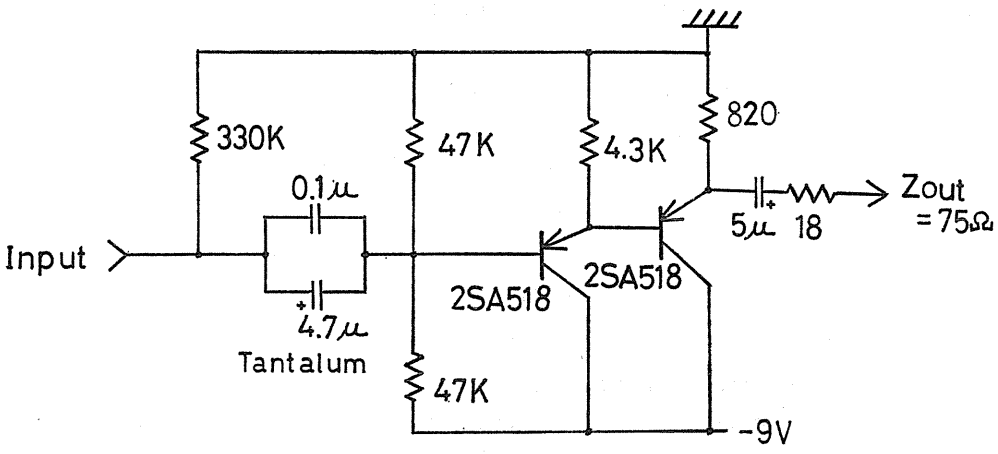

Fig. 4. Emitter Follower Used in Diffusion Length Measurement.

in later sections.

A block diagram of the counting system used is given in Fig. 3, The emitter follower illustrated in Fig. 4 was placed after the preamplifier (PA-20C) for impedance matching. Its output inpedance was adjusted to 75 ohm.

Ⅳ—3. *Measurement and Raw Data*[26]

A hundred channels out of 400 available channels of the pulse-height analyzer were used in the measurement. In order to cut off noise component in the pulse height distribution, the counts in the 6th through 100th channels were summed and used as the count n's in the following, while those in the first through 5th channels were discarded. An Am—Be source of 1 Curie was placed along the center axis, 55 cm from the bottom surface. The coordinates of this position are $x_0=y_0=z_0=0$.

We cannot avoid detecting epi-thermal neutrons by BF_3 detector in such an arrangement. They are the neutrons with energy in 0.5 ~ 10 eV range, and are extraneous for our objective. To circumvent this difficulty there is a well established procedure of cadmium difference method.[34],[35],[36],[37] Measurements were made with and without a cadmium cover around the BF_3 detector. A 0.55 mm thick cadmium cylinder, into which the detector is inserted, cuts down thermal neutron components roughly to a thousandth. By processing the two sets of counts as illustrated below, we obtain net counts for thermal neutrons. Since our objective is to observe relative attenuation of the flux along z-axis, we did not include various correction factors usually applied in absolute measurement.

Suppose we take the following data:

n_b^{Bare}, n_b^{Cd} = Background counts with bare and Cd-covered detector, respectively.

t_b^{Bare}, t_b^{Cd} = Counting time spent for n_b^{Bare}, and n_b^{Cd}.

$n_s^{Bare}(z)$, $n_s^{Cd}(z)$ = Counts taken at z cm from Am—Be (1 Curie) source with bare and Cd-covered detector, respectively.

t_s^{Bare}, t_s^{Cd} = Counting time spent for $n_s^{Bare}(z)$, and $n_s^{Cd}(z)$.

The net counting rate $r_{th}(z)$ due to thermal neutrons which we seek can be given by

$$r_{th}(z)=r_{tot}(z)-r_{epi}(z)\pm\sigma_{th}, \qquad (\text{Ⅳ}-3)$$

where

$$r_{tot}(z)\equiv\{n_s^{Bare}(z)/t_s^{Bare}\}-\{n_b^{Bare}/t_b^{Bare}\}, \qquad (\text{Ⅳ}-4)$$

$$r_{epi}(z)\equiv\{n_s^{Cd}(z)/t_s^{Cd}\}-\{n_b^{Cd}/t_b^{Cd}\}, \qquad (\text{Ⅳ}-5)$$

$$\sigma_{th}^2\equiv\sigma_{tot}^2+\sigma_{epi}^2, \qquad (\text{Ⅳ}-6)$$

$$\sigma_{tot}^2\equiv\{n_s^{Bare}(z)/(t_s^{Bare})^2\}+\{n_b^{Bare}/(t_b^{Bare})^2\}, \qquad (\text{Ⅳ}-7)$$

$$\sigma_{epi}^2\equiv(n_s^{Cd}(z)/(t_s^{Cd})^2\}+\{n_b^{Cd}/(t_b^{Cd})^2\}. \qquad (\text{Ⅳ}-8)$$

The quantity $r_{tot}(z)$ is the count rate due to whole neutron flux (thermal+epi-

thermal) ; $r_{epi}(z)$ is that due to epi-thermal flux. σ_{th} is standard deviation of $r_{th}(z)$. It turned out that $n_b^{Bare} \gg n_b^{Cd}$, which indicates high thermal neutron background in the laboratory.

After obtaining $r_{th}(z)$ (cps), we devide the values by the sensitivity ε (=2.84) of the counter to obtain the Table Ⅱ. The background counting data used in the calculations are

$$n_b^{Bare}=29,738, \quad t_b^{Bare}=390 \text{ min},$$

$$n_b^{Cd}=326, \quad t_b^{Cd}=370 \text{ min}.$$

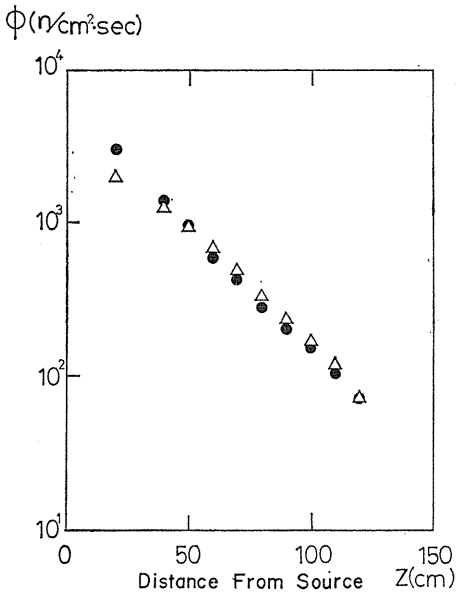

Fig. 5. Thermal Neutron Flux before and after the Correction
△ : the flux before correction
● : the flux after the correction $C_e^{11} \cdot C_h$ is applied [Eq. (Ⅳ—13)].

Table Ⅱ. Thermal Neutron Flux along z-axis [Based on sensitivity ε=2.84 cps/(neutrons/cm²-sec)]

z (cm)	$\phi_{th}(z)$ (n/cm²·sec)
20	$2.003 \pm 0.002 \times 10^3$
40	$1.286 \pm 0.002 \times 10^3$
50	$9.571 \pm 0.017 \times 10^2$
60	$6.926 \pm 0.009 \times 10^2$
70	$4.894 \pm 0.012 \times 10^2$
80	$3.423 \pm 0.010 \times 10^2$
90	$2.378 \pm 0.008 \times 10^2$
100	$1.709 \pm 0.006 \times 10^2$
110	$1.108 \pm 0.003 \times 10^2$
120	$7.219 \pm 0.022 \times 10^1$

Depending on the detector position, the counting time t_s^{Bare} and t_s^{Cd} were varied so that enough counts could be accumulated. The values t_s^{Bare} varied from 2 to 9 minuites, while t_s^{Cd} from 52 to 210 min. The values in Table Ⅱ are illustrated in Fig. 5 by triangles.

Ⅳ—4. *Data Processing*

Now we are in a position to discuss corrections based on Eq. (Ⅲ—44). Considering our specific experimental set-ups, we simplify Eq. (Ⅲ—44) further and carry out iterative corrections. The following are the values which will be used in the procedures.

Average energy of source neutron=5.0 Mev.[38]

τ_{th} (Age of 5.0 Mev neutron in graphite) $=\begin{cases}471\ \text{cm}^2 & \text{for density of } 1.60\ \text{gm/cm}^3,\\ 389\ \text{cm}^2 & \text{for density of } 1.76\ \text{gm/cm}^3.\end{cases}$

The breakdown of this value is as follows:

τ (5.0 MeV $\rightarrow$ 2.0 MeV) $=103$ cm^2 ($\rho=1.60$ gm/cm^3),
[from numerical calculation with Ref. (39)],
τ (2.0 MeV $\rightarrow$ 1.45 eV) $=311$ cm^2 [$\rho=1.60$ gm/cm^3, Ref. (40)],
τ (1.45 eV $\rightarrow$ thermal energy) $=57$ cm^2 [$\rho=1.60$ gm/cm^3, Ref. (40)].
d (extrapolation distance) $=1.8$ cm,
a=b=153.6 cm, c=203.6 cm,
$\mu_1=56.8$ cm, $\mu_2=146.8$ cm.

To write down (Ⅲ—43) in a form convenient for our purpose, we have

$$\phi_{app}(x,\ y,\ z)=\frac{S_0\exp(\tau_{th}/L^2)}{4D}\cdot\sum_{k,\,l}\frac{F_{kl}(x,\ x_0\,;\ y,\ y_0)}{\alpha_{kl}}\,\frac{\exp(-\alpha_{kl}z)A_{kl}J_{kl}(z)}{C_e^{kl}(z)} \qquad (\text{Ⅳ}-9)$$

where

$$F_{kl}(x,\ x_0\,;\ y,\ y_0)=X_k(x_0)X_k(x)Y_l(y_0)Y_l(y),$$

$$A_{kl}=1-\exp(-2\alpha_{kl}\mu_1),$$

$$C_e^{kl}(z)=\{1-e^{-2\alpha_{kl}(\mu_2-z)}\}^{-1} \qquad \text{(end correction)},$$

$$\begin{aligned}J_{kl}(z)=1+A_{kl}^{-1}\cdot\{&\operatorname{erf}[(z/2\sqrt{\tau_{th}})-\alpha_{kl}\sqrt{\tau_{th}}]-\\&-\exp(-2\alpha_{kl}\mu_1)\operatorname{erf}[(z+2\mu_1)/2\sqrt{\tau_{th}}-\alpha_{kl}\sqrt{\tau_{th}}]+\\&+C_e^{kl}(z)\exp(2\alpha_{kl}z)[1-\exp[-2\alpha_{kl}(\mu_1+z)]]\cdot\\&\cdot[1-\operatorname{erf}[(z/2\sqrt{\tau_{th}})+\alpha_{kl}\sqrt{\tau_{th}}]]\}.\end{aligned} \qquad (\text{Ⅳ}-10)$$

In deriving (Ⅳ—9) we have employed approximations

$$\sinh\alpha_{kl}c\ \approx\ \exp(\alpha_{kl}c)/2,$$

$$\exp(-2\alpha_{kl}\mu_2)\ll 1,$$

$$\operatorname{erf}[(z+2\mu_1)/2\sqrt{\tau_{th}}]\ \approx\ 1,$$

which are valid for the range of values listed above. Since we are interested in a form of single exponential decay, we put (Ⅳ—9) in the following form:

$$\phi_{app}(x,\ y,\ z)=\frac{S_0\exp(\tau_{th}/L^2)}{4\bar{D}}\cdot$$

$$\cdot\frac{F_{11}}{\alpha_0}A_{11}C_e^{11}(z)^{-1}\exp(-\alpha_0 z)C_h^{-1}(z), \qquad (\text{Ⅳ}-11)$$

where $C_h(z)$, harmonic correction factor, is given by

$$C_h^{-1}(z)=J_{11}(z)+\sum_{(k,l)\neq(1,1)}\frac{F_{kl}}{F_{11}}\frac{\alpha_0}{\alpha_{kl}}\frac{C_e^{11}(z)}{C_e^{kl}(z)}\frac{A_{kl}}{A_{11}}J_{kl}(z)\exp[-(\alpha_{kl}-\alpha_0)z]. \qquad (\text{Ⅳ}-12)$$

Rearranging Eq. (Ⅳ—11), and taking its logarithm, we derive a working formula

$$\ln[\phi_{app}(x,\ y,\ z)C_e^{11}(z)C_h(z)]=\text{Const}-\alpha_0 z. \qquad (\text{Ⅳ}-13)$$

The iterative procedure is as follows: we make a guess on the value of L, and hence of α_0, and use it for evaluation of $C_e^{11}(z)$ and $C_h(z)$ on the left side of (Ⅳ—13). These correction factors are multiplied by $\phi_{th}(z)$ of Table Ⅱ, and plotted on a semi-log sheet. From the slope of the curve we read α_0, the value for the next iteration. Then the left side of (Ⅳ—13) is recalculated, and so forth. The procedure converged after two iterations. The final corrected points are illustrated by dark dots in Fig. 5.

In evaluating the function $J_{kl}(z)$ of (Ⅳ—10), the product $\exp(2\alpha_{kl}z)\{1-\text{erf}[(z/2\sqrt{\tau_{th}})+\alpha_{kl}\sqrt{\tau_{th}}]\}$ in its last term can be approximated by an asymptotic expansion[41]

$$1-\text{erf}(t)\approx[\sqrt{\pi_t}\,t\,\exp(t^2)]^{-1}\{1-(1/2t^2)\}.$$

Further, depending on the values of z, the error functions in other terms of $J_{kl}(z)$ may be put equal to unity. In the range of z values in Table Ⅱ, $C_e{}^{11}(z)$ varied from unity to 1.18, whereas $C_h{}^{-1}(z)$, from 1.12 to 2.00.

The final iteration led to the value

Table Ⅲ. Comparison of Diffusion Length Measurements
(all values are normalized for $\rho=1.60$ gm/cm^3)

Author		L (cm)	References
Richey and Block		54.2±0.6	Ref. (6)
Carlblom		46.8±0.2	Table 17. 1. 4. of Ref. (25)
Antonov et al		51.1±2.1	Ref. (75)
Present Measured Value		49.2±0.8	
CALCULATED	Pure graphite	61.6	Based on Ref. (33)
	With 0.039 PPM of Boron	61.3	〃
	With 1 PPM of Boron	55.1	〃
	With 2.55 PPM of Boron	49.2	〃

$$L_{1.76}=44.7\pm0.7 \text{ cm for } \rho=1.76 \text{ gm/cm}^3. \quad (\text{Ⅳ}-14)$$

If corrected for density, it gives

$$L_{1.60}=49.2\pm0.8 \text{ cm for } \rho=1.60 \text{ gm/cm}^3. \quad (\text{Ⅳ}-15)$$

The values are compared in Table Ⅲ with literature values.

Ⅳ—5. *Discussions*

The values in Table Ⅲ distribute over fairly wide range, namely with differences near 15 %. The values in literatures do not give contents of impurity in graphite, and such contents can be a source of disagreement. Therefore our value should rather be taken as a calibration value for this specific batch of the material. In the table an attempt was made to attribute the discrepancy between our value and that calculated from Ref. (33) to the contents of boron. If this was the only source of the difference the content has to be 2.55 ppm.

However, there can be other sources of error. The first is the effect of void space around the detector. Since Type J block was used for detector cavity, there was 7 mm-wide annular void space between the detector and graphite. Other possible sources are (1) neutrons being reflected from room walls, (2) moisture held in graphite, (3) error of age theory for penetrating neutrons, that is, for the positions far from the source, (4) anisotropic neutron flux near the source for which age-diffusion theory is not valid, (5) insufficient curve fitting, (6) inadequate value of τ_{th} used in data processing. The question of impurity will be discussed again later in connection with pulsed neutron experiment.

Ⅴ. Condition for Existence of Diffusion Length

The measurement described in Sec. Ⅳ was carried out with the assumption that an attenuation mode of $\exp(-\alpha_0 z)$ is included in the flux distribution. According to the assumption, the harmonic correction $C_h(z)$ would approach a constant for z sufficiently away from the source, if the stack is long enough in z-direction. At the same time, the end correction $C_e{}^{kl}(z)$ would become unity for detector positions sufficiently far inside the other end of the stack. Thus one would be able to find a region of single exponential decay well inside the stack.

It was gradually revealed during 1960's that this assumption does not hold for every case. If the transverse dimension of a stack is too small, such an attenuation mode does not exist. This is a conclusion out of neutron thermalization theories which were developped mainly from 1962 through 1967, and which employed energy-dependent diffusion equation or transport equation.[20],[19],[21],[16] In this review we introduce the theory of Williams[3] on diffusion length. The proof will be on intuitive basis rather than mathematical rigor.

We return to the case of an infinite prism shown in Fig. 1. Sufficiently away from an external source plane (say, five times neutron mean free path), energy dependent neutron flux is composed of secondary neutrons being scattered at least once, and the component directly coming from the source can be negligible. Then the following form of integral transport equation applies:[42]

$$\phi(x,\ y,\ z,\ E)=\int_0^\infty dE'\sum_s(E'\to E)\int_{-a/2}^{a/2}dx'\int_{-b/2}^{b/2}dy'\int_{-\infty}^{\infty}dz'\phi(x',\ y',\ z',\ E')$$
$$\cdot\exp\{-\sum_t(E)\sqrt{\Delta^2+w^2}\}/4\pi\{\Delta^2+w^2\},\qquad(\text{V}-1)$$

where, $\Delta^2=(x-x')^2+(y-y')^2$, $w^2=(z-z')^2$, and where $\phi(x,\ y,\ z,\ E)$ is energy-dependent total neutron flux at a point $(x,\ y,\ z)$, obtained by integrating angular flux over solid angle. Isotropic scattering is assumed. The function $\sum_s(E'\to E)$ is called scattering kernel whose unit is [cm^{-1}. ev^{-1}], and is proportional to the probability of a neutron being scattered at energy E' and transfered to energy E.[43] The integrand on the right side of (V—1) expresses [reaction rate of this energy transition] × [the probability of the neutron being scattered toward the point $(x,\ y,\ z)$] × [spatial attenuation].

Now we assume that neutron flux forms cosine distributions in x-y directions, and attenuates along z-axis by $\exp(-Qz)$. Such a distribution was assumed in every $(k,\ l)$ mode in the treatment of Sec. IV. We now assume fundamental (1, 1) mode and seek a necessary condition for this distribution. The analogous conditions for higher modes could easily be obtained afterwards. Thus we put

$$\phi(x,\ y,\ z,\ E)\equiv\varphi_0(B_x,\ B_y,\ Q,\ E)\exp\{i(B_xx+B_yy)-Qz\},$$

and substitute it into (V—1). The result is

$$\varphi_0(B_x,\ B_y,\ Q,\ E)=\int_0^\infty\frac{dE'\sum_s(E'\to E)}{4\pi}\varphi_0(B_x,\ B_y,\ Q,\ E')f(E),\quad(\text{V}-2)$$

where

$$f(E)\equiv\int_{-\infty}^{\infty}dw\int_{-a/2-x}^{a/2-x}du\int_{-b/2-y}^{b/2-y}dv\ \exp\{(B_xu+B_yv)-Qw\}$$
$$\cdot\exp\{-\sum_t(E)\sqrt{u^2+v^2+w^2}\}\{u^2+v^2+w^2\}^{-1},\qquad(\text{V}-3)$$

and where

$$u=x'-x,\quad v=y'-y,$$

and

$$B_x=\pi/a,\quad B_y=\pi/b.\qquad(\text{V}-4)$$

In the above expression of $f(E)$, definite limits of integration such as $a/2-x$ are given for variables u and v. However, we can extend these limits to infinity according to asymptotic reactor theory, which is an approximate method of solution.[44],[45] To briefly state the context, the theory says that neutron flux distribution within a finite system can be given by the corresponding part of a solution for an extended infinite medium problem, which becomes zero at the extrapolated boundary of the given finite system. It has been shown that if the flux within the finite system can be written as a sum of eigenfunctions of wave equation $((\nabla^2+k_n^2)\ g_n(\underline{x})=0)$, this theory is strictly valid.[45] In many cases neutron flux within a system forms coine distribution well inside the surface, and thus such an asymptotic theory has great advantage. In our case, we have assumed exp $(iB_xx+$

$iB_y y$) form, and therefore this extension of integration limits is valid in x and y directions. Then the integration in (Ⅴ—3) can be carried out over three-dimensional infinite space, and can be expressed by spherical co-ordinates as

$$f(E)=\int_0^{2\pi} d\varphi \int_0^{\pi} \sin\theta\, d\theta \cdot$$

$$\int_0^{\infty} d\rho \exp\{\rho[i\sin\theta \cdot B_\perp \cos(\varphi-\beta)-(\Sigma_t+Q\cos\theta)]\}, \qquad (Ⅴ—5)$$

where the following changes of variables have been applied:

$$\left.\begin{aligned} &u\equiv\rho\sin\theta\cos\varphi,\\ &v\equiv\rho\sin\theta\sin\varphi,\\ &w\equiv\rho\cos\theta,\\ &B_\perp\equiv\sqrt{B_x^2+B_y^2}=B_{11}\quad[cf.\ (Ⅲ—17)],\\ &\tan\beta=B_x/B_y. \end{aligned}\right\} \qquad (Ⅴ—6)$$

Before we carry out integration over ρ, we point out that the value of Q is such that

$$Q\leq \mathrm{Min}[\Sigma_t(E)] \qquad (Ⅴ—7)$$

on physical ground: if not, then in certain energy for which Q exceeds $\Sigma_t(E)$, the exponential factor in (Ⅴ—3) diverges when $u=0$, $v=0$, $w<0$. Physically this should not occur. Thus integration over ρ in (Ⅴ—5) leads to a result

$$f(E)=\int_0^{\pi}\sin\theta\, d\theta \int_0^{2\pi}\frac{d\varphi}{(\Sigma_t+Q\cos\theta)-iB_\perp\sin\theta\cos(\varphi-\beta)}. \qquad (Ⅴ—8)$$

The integration over φ is in a form

$$I=\int_0^{2\pi}\frac{d\varphi}{A_1+iA_2\cos(\varphi-\beta)},$$

where $A_1>0$, $A_2<0$. This integration can be carried out in general by a change of variable $S=e^{i\varphi}$, which transforms I into a form

$$I=\frac{-2\exp(i\beta)}{A_2}\cdot\oint_{\text{unit circle}}\frac{dS}{S^2-(2A_1/A_2)i\exp(i\beta)S+\exp(2i\beta)}. \qquad (Ⅴ—9)$$

Out of two poles, the one at

$$S^*=i\exp(i\beta)\{A_1/A_2+\sqrt{1+A_1^2/A_2^2}\} \qquad (Ⅴ—10)$$

is inside the unit circle. By residue calculation for this pole, we obtain the result

$$I=\frac{2\pi}{\sqrt{(\Sigma_t(E)+Q\cos\theta)^2+B_\perp^2\sin^2\theta}}. \qquad (Ⅴ—11)$$

Substitute this result into (Ⅴ—8), and integrate over $t=\cos\theta$. The final result can be simplified if we define a constant

$$\nu^2 \equiv Q^2 - B_\perp^2. \qquad (Ⅴ—12)$$

Then $f(E)$ becomes

$$f(E) = \frac{2\pi}{\nu} \ln\left\{ t + \frac{\sum_t(E)Q}{\nu^2} + \sqrt{t^2 + \frac{2\sum_t(E)Q}{\nu^2} t + \frac{B_\perp^2 + \sum_t^2(E)}{\nu^2}} \right\}\Bigg|_{t=-1}^{1}$$

$$= \frac{2\pi}{\nu} \ln \frac{\sum_t(E)+\nu}{\sum_t(E)-\nu} \qquad (Ⅴ—13)$$

and Eq. (Ⅴ—2) for $\varphi_0(B_x, B_y, Q, E)$ takes the form

$$\varphi_0(B_x, B_y, Q, E) = \frac{1}{2\nu} \ln \frac{\sum_t(E)+\nu}{\sum_t(E)-\nu} \cdot \int_0^\infty dE' \sum_s(E' \to E) \varphi_0(B_x, B_y, Q, E'). \qquad (Ⅴ—14)$$

This is exactly in the same form as the energy-dependent transport equation for one-dimensional problem, where a plane source is placed within infinite medium. The latter problem is nothing but the diffusion length problem of Sec. Ⅲ. If one assumes one-dimensional attenuation of $\exp(-z/L)$, and substitutes it into transport equation, as the result the eigenvalue $1/L$ obeys the same equation as Eq. (Ⅴ—14), with ν replaced by $1/L$. By solving such an equation one can obtain more rigorous value of L than that by diffusion equation. The equations for the two problems being the same, ν in Eq. (Ⅴ—14) is equal to the inverse of diffusion length, and $\varphi_0(B_x, B_y, Q, E)$ is the same as energy spectrum of infinite medum diffusion length experiment.

Williams[3] interprets this relation as follows: The transverse cosine distribution gives rise to transverse leakage, and results in cooling of the spectrum, while the attenuation in z-direction by $\exp(-\nu z)$ causes heating. These two components are in balance, and results in the same energy spectra as infinite medium solution.

Replacing ν in Eq. (Ⅴ—12) by $1/L$ we then have a relation,

$$Q^2 = \frac{1}{L^2} + B_\perp^2. \qquad (Ⅴ—15)$$

On the other hand we have a restriction on Q as Eq. (Ⅴ—7). By combining these two equations we are led to a necessary condition

$$B_\perp^2 \leq \{\mathrm{Min}[\sum_t(E)]\}^2 - \frac{1}{L^2} \qquad (Ⅴ—16)$$

for existence of the decay mode $\exp(-Qz)$. The inequality puts a restriction on the transverse size of the prism through $B_\perp^2$ defined by (Ⅴ—4) and (Ⅴ—6). According to the foregoing explanations by Williams, the balance in energy spectrum breaks down beyound this limit because of too much transverse leakage.

The required minimum size varies from material to material. For graphite of 300° K, the minimum of microscopic total cross section is observed at 1.5 meV to

be Min $[\sigma_t(E)]=0.55$ barn.[39] With the density of 1.76 gm/cm^3, the minimum is reflected upon total cross section as Min $[\Sigma_t(E)]=4.85\times10^{-2}$cm^{-1}. Assuming the diffusion length of 45 cm to 50 cm for this density of graphite we obtain

$$(B_\perp^2)\leq 1.86\sim1.95\times10^{-3}\text{cm}^{-2}, \qquad (\text{V}-17)$$

$$a=b\geq 103\sim101\text{ cm}, \qquad (\text{V}-18)$$

where we assumed $a=b$. Therefore our graphite stack, whose extrapolated transverse dimension is $a=b=153.6$ cm, is well above this limit.

We have shown by intuitive discussions (transverse cosine distribution, asymptotic reactor theory, and analogy from one-dimensional problem) that there exists a minimum transverse dimension required in this kind of experiment, and confirmed the validity of our experimental set-up. Williams' another proof[3] is based on more rigorous derivations, and concludes that the maximum chord length of cross-sectional area on x-y plane has to be larger than a certain value which depends on the scattering kernel $\Sigma_s(E'\to E)$. The present proof is more convenient in experiments than such a rigorous version in that the conclusion gives the minimum system size more directly.

We note also that there is an analogous requirement which puts an upper limit on absorption cross section. Moreover, a similar requirement can be cosidered for an exponential-decay experiment on multiplying medium which includes nuclear fuel.

VI. Theory of Pulsed-Neutron Experiment

We go on to the report of pulse decay experiment which was carried out at our laboratory. Pulse decay experiment in moderator determines the average diffusion coefficient $\bar{D}$ and average macroscopic absorption cross section $\bar{\Sigma}_a$ of thermal neutrons, while diffusion length measurement determines $\bar{D}/\bar{\Sigma}_a$. If applied to a nearly critical multiplying system, pulsed neutron method determines the magnitude of deviation from criticality, which is called reactivity.[46] We confine our present discussion on moderator experiment.

VI—1. *One-speed Theory*

We start with one-speed time-dependent diffusion equation

$$\bar{D}\nabla^2\phi_T(x,\ t)-\bar{\Sigma}_a\phi_T(x,\ t)+S(x,\ t)=\frac{1}{v}\frac{\partial\phi_T}{\partial t}. \qquad (\text{VI}-1)$$

The following derivations will be made suitable for the analysis of experiments carried out in a parallelepiped system. Source neutrons of 15 MeV are injected on one side of the system by a neutron generator. These neutrons undergo slowing-down, and form distributed source of thermal neutrons. During the slowing-down process, neutrons leak out of the system, and the probability for a neutron to survive this leakage process is $\exp(-B_{klm}^2\tau_{th})$, as shown in Eq. (III—19).[47],[48] For the source term, therefore, it is usually sufficient to include the fundamental mode and the next level of higher modes, $(k,\ l,\ m)=(1,\ 1,\ 3)$, $(1,\ 3,\ 1)$ and $(3,\ 1,\ 1)$. In the following treatment we only include the fundamental mode, and put the source term as[47]

$$S(\underline{x},\ t)=S_0\delta(t)X_1(x)Y_1(y)Z_1(z). \qquad (\text{Ⅵ}-2)$$

The coordinate system in Secs. Ⅵ and Ⅶ, which will be specified later, is chosen independently from that of Secs. Ⅲ and Ⅳ.

If the fundamental mode is dominant in $S(\underline{x},\ t)$, we can assume that time-dependent thermal flux includes only a fundamental mode as

$$\phi_T(x,t)=a_1(t)X_1(x)Y_1(y)Z_1(z), \qquad (\text{Ⅵ}-3)$$

and arrive at a solution

$$\phi_T(x,\ t)=a_1(0)X_1(x)Y_1(y)Z_1(z)\exp\{-\bar{v}(\bar{\Sigma}_a+\bar{D}B_0^2)t\}, \qquad (\text{Ⅵ}-4)$$

where

$$B_0^2\equiv B_{111}^2 \quad [\text{cf. Eqs. } (\text{Ⅱ}-4) \text{ and } (\text{Ⅲ}-21)].$$

In justifying this derivation we add that higher mode contamination of counting data can be eliminated by proper positioning of detector, and by waiting long enough for the fundamental mode to become dominant, as higher modes decay faster. Thus the decay constant is given by

$$\lambda=\bar{v}(\bar{\Sigma}_a+\bar{D}B_0^2), \qquad (\text{Ⅵ}-5)$$

where

$$\bar{v}=\int_0^\infty vn(E)\,dE\Big/\int_0^\infty n(E)\,dE=(2/\sqrt{\pi})\sqrt{2kT_n/m}, \qquad (\text{Ⅵ}-6)$$

and where $n(E)$ is thermal neutron energy distribution. The last result assumes Maxwellian distribution of temperature T_n for neutrons of mass m. With various sizes of the system we carry out pulse decay experiments, and determine λ's for each B_0^2. By drawing a λ vs. B_0^2 curve, we determine $\bar{v}\bar{\Sigma}_a$ and $\bar{v}\bar{D}$: the former is read from the intersection of the curve with λ-axis, and the latter from the slope.

Ⅵ—2. *Improvement of the Treatment by Energy-Dependent Equation*

We can improve the above theory by including energy variable in the equation.[15] It is too lengthy to be reproduced here, and we give only its conclusion. According to the theory, the result (Ⅵ—5) has to be modified as[49],[15],[47]

$$\lambda=\bar{v}\bar{\Sigma}_a+D_0B_0^2-CB_0^4 \qquad (\text{Ⅵ}-7)$$

where

$$D_0\equiv\bar{v}\bar{D}. \qquad (\text{Ⅵ}-8)$$

The constant C takes account of temperature fall due to leakage, and is called diffusion-cooling coefficient. The temperature fall is given by

$$\frac{T_n-T_m}{T_m}\cong-2B_0^2C/(\bar{v}\bar{D}). \qquad (\text{Ⅵ}-9)$$

According to Beckurts,[49] C is given as

$$C=\bar{v}(\bar{D})^2(1+2R)^2/(2M_2^*), \qquad (\text{VI}-10)$$

$$M_2^*=(kT_n)^{-2}\int_0^\infty dE'\int_0^\infty dE M(E',\ T_n)\Sigma_s(E'\to E)(E'\to E)^2, \qquad (\text{VI}-11)$$

where the function $M(E,\ T_n)$ is that given by (III—5).

As one can see from the expression (VI—11), M_2^* is the second moment of energy transfer per sec., and therefore a measure of energy exchange between neutrons and moderator atoms. The constant R expresses the degree of D variation due to temperature change, and can be set equal to zero for graphite.[49]

To summarize, diffusion cooling is an effect caused by preferential loss of those neutrons which have larger velocities. The loss of higher energy side of thermal spectrum reduces the value of $\bar{v}$ within the system, and the pulse decay is also reduced because the decay depends on $\bar{v}$. The third term of (VI—7) expresses such reduction of decay process. The more energy is exchanged between neutrons and medium, the larger value of M_2^* results, which in turn lowers C value and hence less cooling. In other words, intense collisions between neutrons and moderator nuclei make up for the cooling effect, and the decay of the pulse almost follows the manner predicted by (VI—5), which is based on Maxwellian equilibrium spectrum.

VII. Experiment of Pulsed-Neutron at Nuclear Engineering Department

To verify such theoretical conclusions, pulse experiment was carried out during the summer, 1971, with the graphite blocks previously described. The experimental set-ups are (1) graphite stack, (2) neutron source, (3) beam controlling circuits,

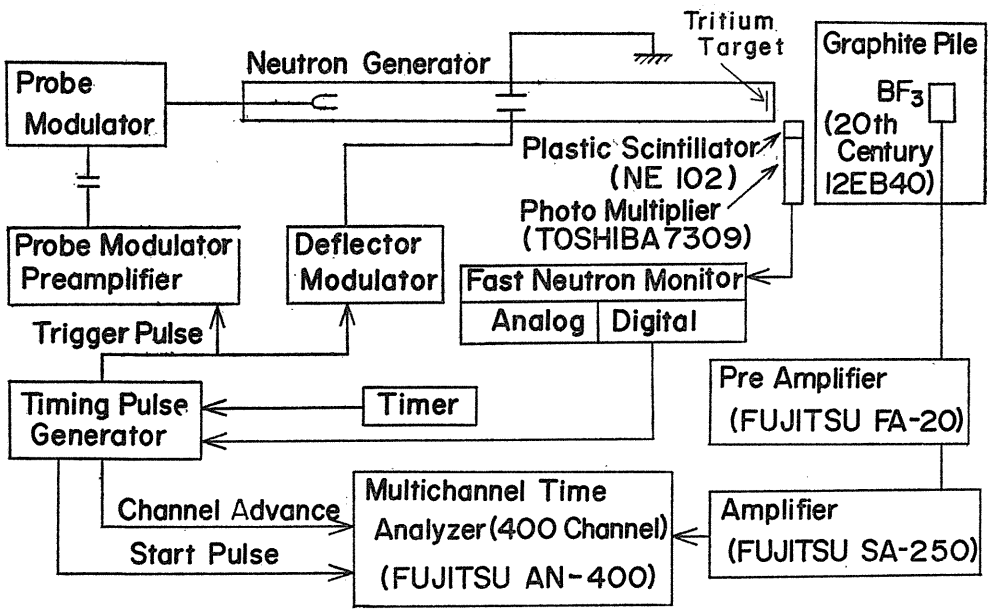

Fig. 6. Block Diagram of Experimental Set-up for Pulsed-Neutron Experiment.

(4) neutron detectors, and (5) counting systems. The description of these components will be presented first in the following. The overall block diagram of these components are given in Fig. 6.

Ⅶ—1. *Experimental Set-up*

(1) *Graphite Stack*

The graphite which was manufactured by Showa Denko, and described in Sec. Ⅳ—1, was used to construct various sizes of parallelepiped system. Sixteen sizes tabulated in Tabel. Ⅳ were investigated. The extrapolation distance $d=1.8$ cm (for

Table Ⅳ. Various Sizes of Graphite Stack Investigated by Pulsed-Neutron Technique

Stack Identification No.	Dimensions(*1) $a_0\times b_0\times c_0$ (cm^3)	Buckling(*2) B^2 (cm^{-2})
B_1	150×150×200	1.074×10^{-3}
B_2	150×150×150	1.255
B_3	150×150×100	1.756
B_4	150×100×100	2.257
B_5	100×100×100	2.758
B_6	100×100× 70	3.661
B_7	100×100× 60	4.279
B_8	100×100× 50	5.274
B_9	100× 70× 50	6.177
B_{10}	100× 60× 50	6.794
B_{11}	100× 50× 50	7.790
B_{12}	90× 50× 50	7.997
B_{13}	80× 50× 50	8.283
B_{14}	70× 50× 50	8.692
B_{15}	60× 50× 50	9.310
B_{16}	50× 50× 50	10.306

(*1) a_0, b_0 and c_0 are the actual physical dimensions excluding extrapolation distance.

(*2) $B_0^2=\pi^2\left[\frac{1}{a^2}+\frac{1}{b^2}+\frac{1}{c^2}\right]$, where $a=a_0+2d$, $b=b_0+2d$, $c=c_0+2d$, and $d=1.80$ cm.

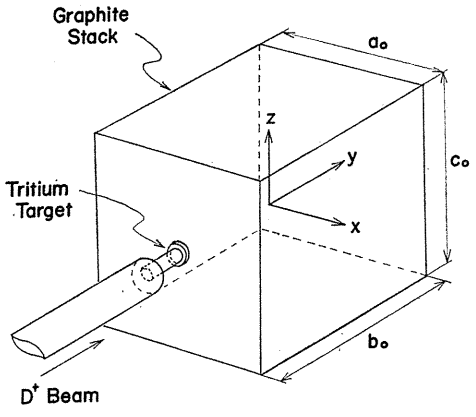

Fig. 7. The Relative Position of Tritium Target with Respect to Graphite Stack, and the Direction of the Sides a_0, b_0 and c_0.

$\rho=1.76\,gm/cm^3$) was used again for the evaluation of buckling, which is based on the value $\sigma_s=4.8$ barn.[33] The directions of x-, y-, z-axes, the sides a_0, b_0, c_0, and their relative positions with respect to the tritium target are illustrated in Fig. 7. The origin is placed at the center of the system, and the target is positioned at $x=0$, $z=0$. Cadmium plates of 0.55 mm thickness covered the surface of the stack so that room return thermal neutrons could be cut-down.

(2) *Neutron Generator*

It is Type NT-20 of Toshiba Electric Co. with accelerating voltage of 200 kV, which was manufactured in February, 1962. It is an accelerator of Cockcroft-Walton type, which accelerates D^+ ion, or D^{++} ion with less quantity. At one end of a beam transport tube, the deuteron beam is focused upon a titanium-coated copper plate of 28.5 mm diameter and 0.5 mm thickness. Tritium is adsorbed upon the titanium layer. The transport tube between this tritium target and the last stage accelerating electrode is 5.70 m long. By reading the voltage across a resistance between the target and the ground, the ion current reaching the target during this series of experiments was estimated to be 80 to 220 micro amps. Neutron yield, which depends on the target wear, was estimated at the time of experiment as 3×10^7 neutrons/sec·μA, which was recently confirmed as reasonable with more reliable means.[50] The nominal yield by the manufacturer is 10^7 to 10^8 neutrons/sec·μA.

The pulse width was set to 180 to 400 micro sec during this experiment. Therefore, a typical neutron yield per pulse is estimated as 1.2×10^6 neutrons/pulse, by assuming a D^+ current pulse of 100 micro amps for a duration of 400 micro sec.

(3) *Beam Controlling Circuits (Pulsing Device)*

Pulsed deuteron beam was generated by simultaneous control of ion extraction

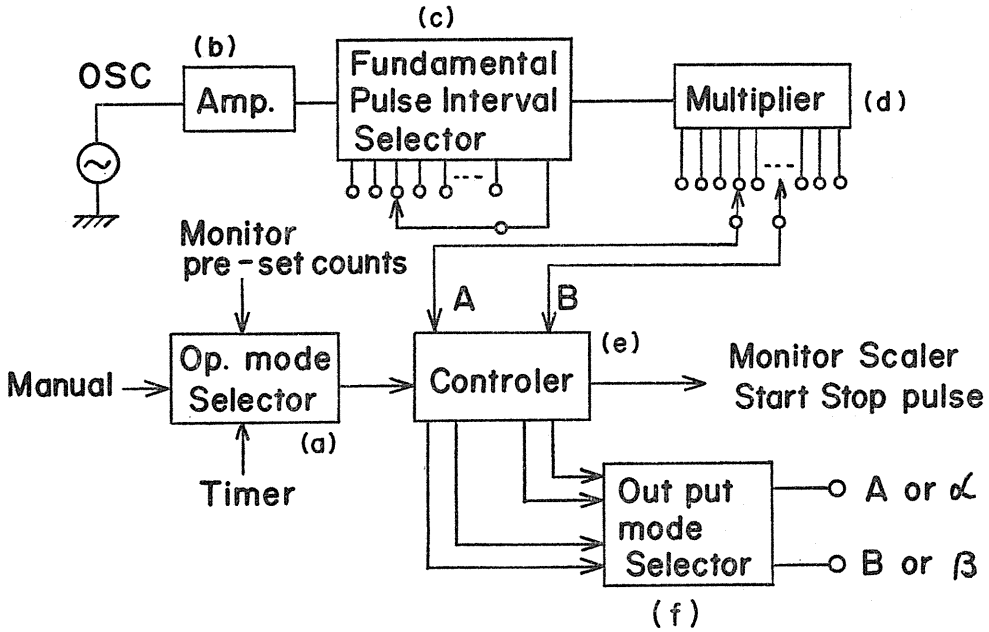

Fig. 8. Timing Pulse Generator Block Diagram

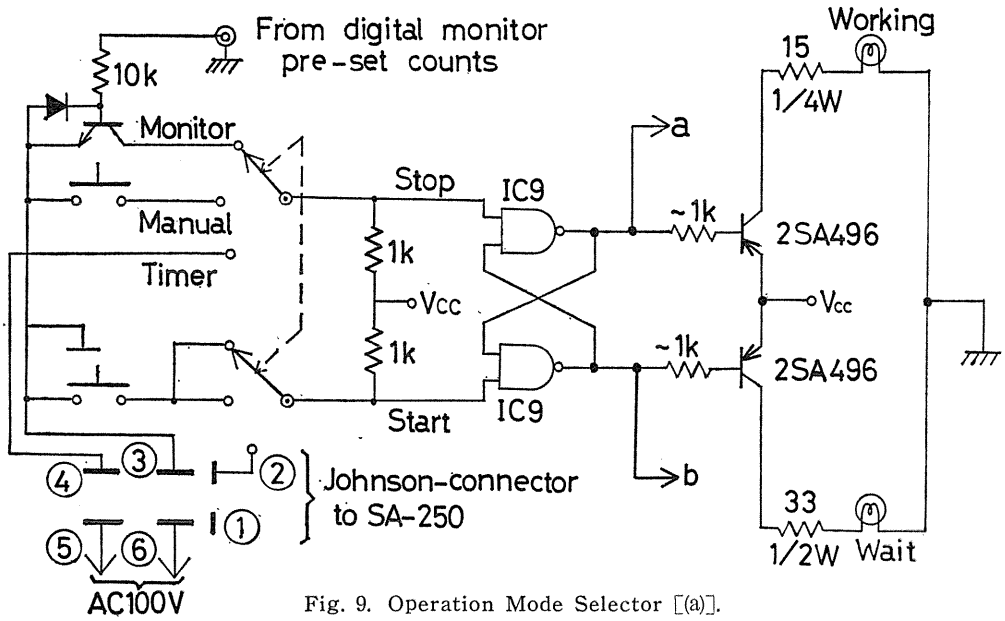

Fig. 9. Operation Mode Selector [(a)].

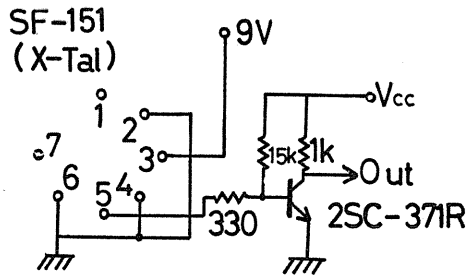

Fig. 10. Oscillator and Amplifier [(b)].

Fig. 11-1 Fundamental Pulse Interval Selector [(c)].

voltage and deflector voltage (4 kV). The timing of these voltage pulses was controlled and administered by Timing Pulse Generator, whose function in connection with other devices can be understood by Fig. 6.

As to the components included in the Timing Pulse Generator (TPG) they are conceptually illustrated in Fig. 8 by their respective functions. The circuits of each component is given in Fig. 9 through Fig. 13. The correspondence between these figures and Fig. 8 is indicated by lower case alphabets: Operation Mode Selector is illustrated in Fig. 9, Oscillator and Amplifier in Fig. 10, Fundamental Pulse Interval Selector in Figs. 11—1, and 11—2, Multiplier in Fig. 12, Controler and Output Mode

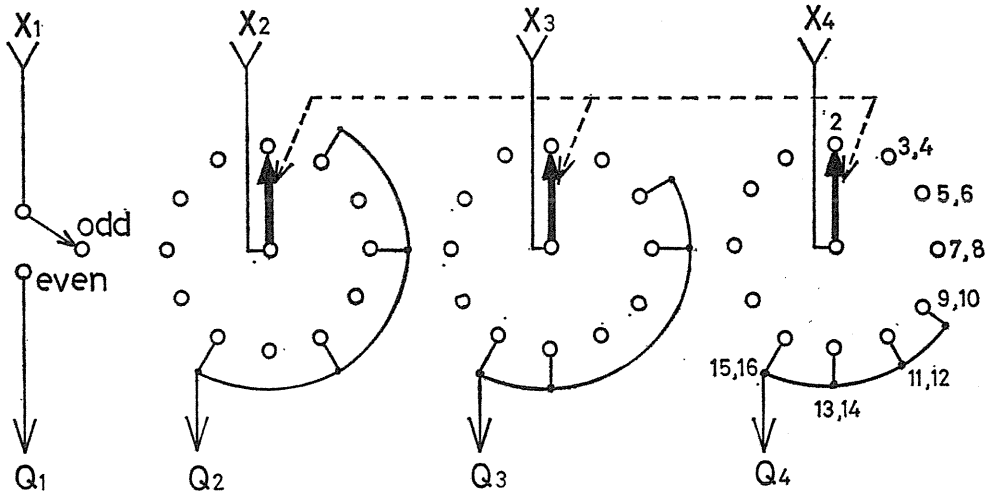

Fig. 11-2. Fundamental Pulse Interval Selector [(c)].

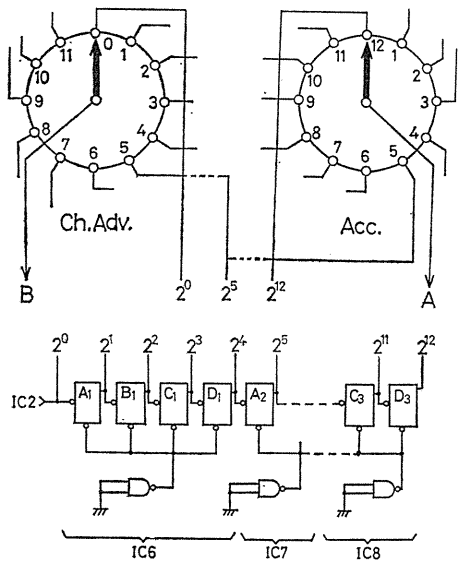

Fig. 12. Multipller [(d)].

Table V. The Integrated Circuits Used in the Timing Pulse Generator

IC No.	
1	TD 3420 P
2	TD 3400 P
3	TD 3400 P
4	TD 3473 P
5	TD 3473 P
6	TD 3493 P
7	TD 3493 P
8	TD 3493 P
9	TD 1065 P
10	TD 1073 P
11	TD 1072 P
12	TD 1065 P
13	TD 1065 P

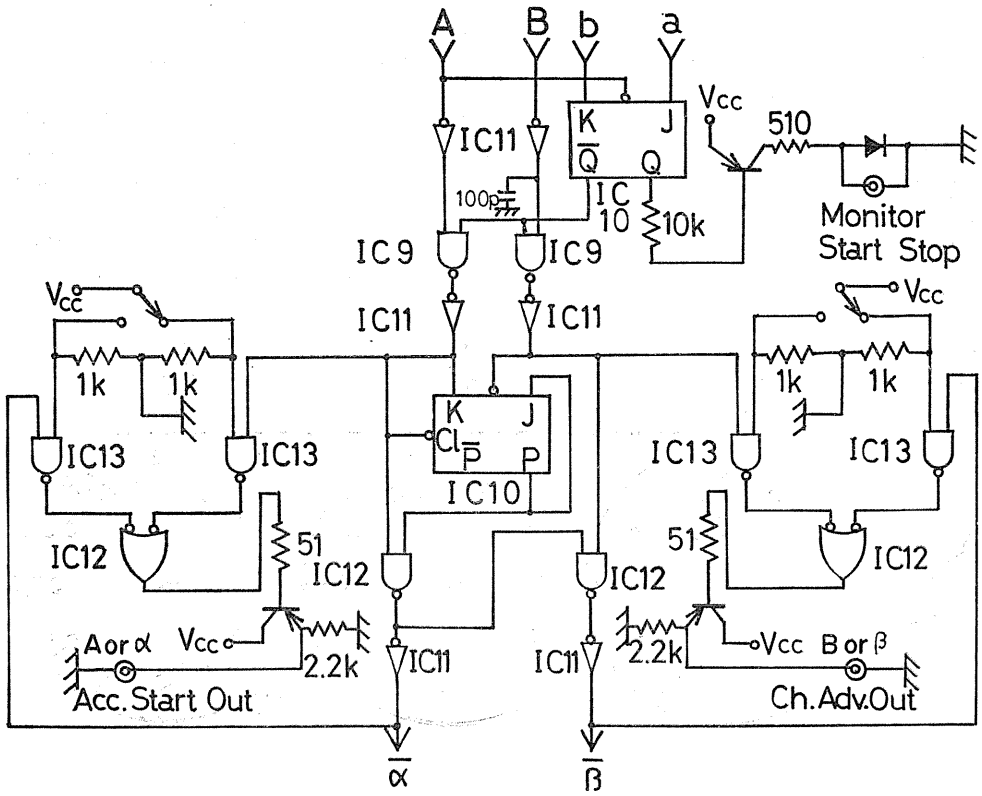

Fig. 13. Controller [(e)] and Output Mode Selector [(f)].

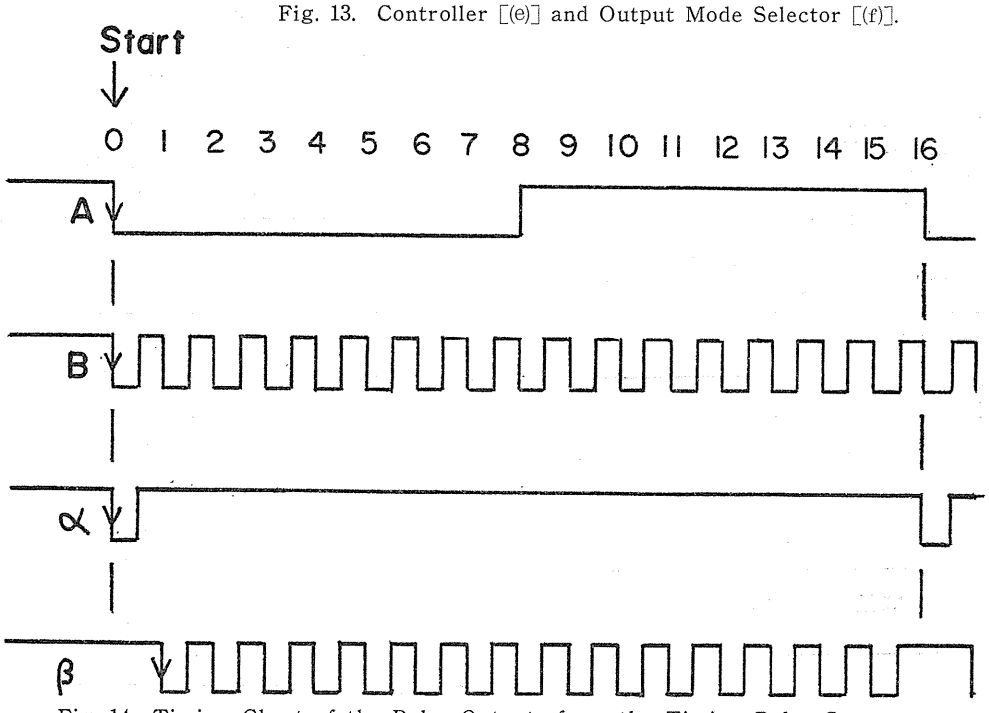

Fig. 14. Timing Chart of the Pulse Outputs from the Timing Pulse Generator.

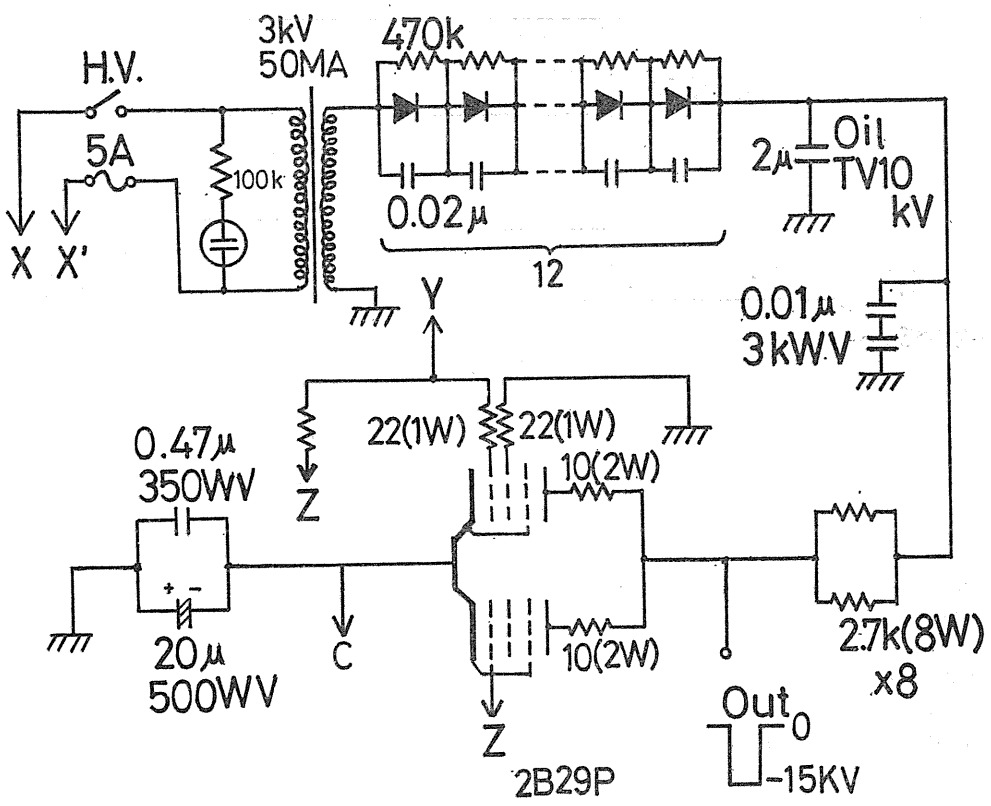

Fig. 15-1. Deflector Modulator (1).

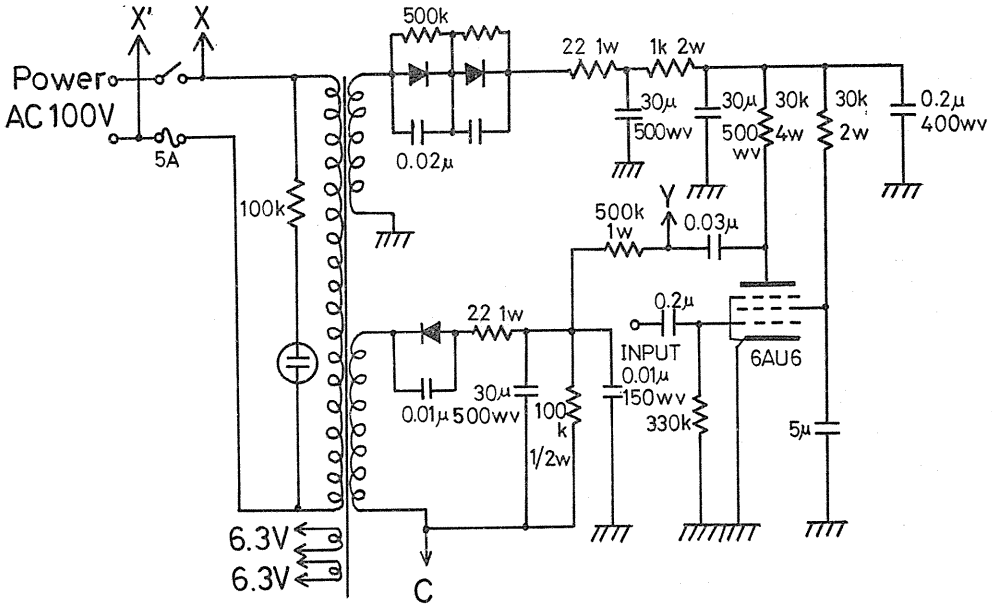

Fig. 15-2. Deflector Modulator (2).

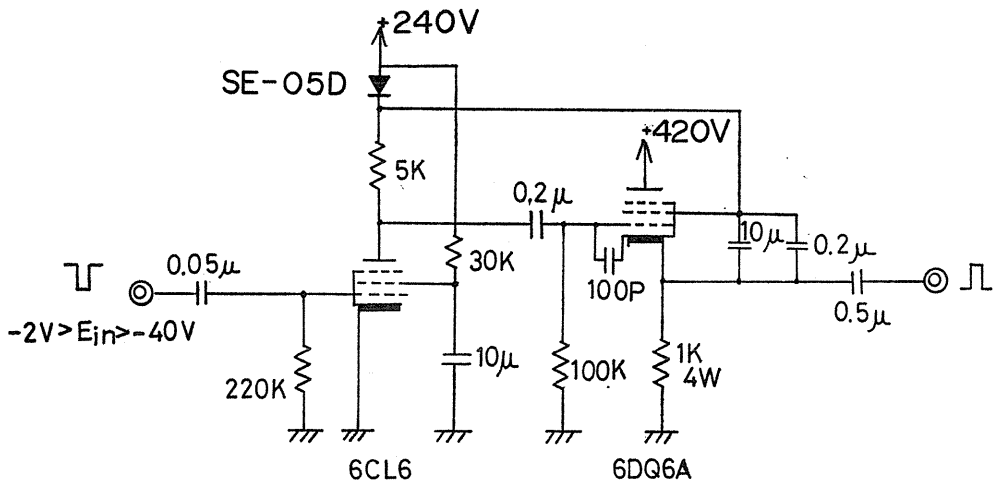

Fig. 16. Probe Modulator Preamplifier

Selector in Fig. 13. The integrated circuits used in the TPG are listed in Table Ⅴ. The timing of pulse outputs from the TPG is illustrated in Fig. 14.

Among other components of Fig. 6, the Deflector Modulator is illustrated in Figs. 15—1 and 15—2, the Probe Modulator Preamplifier in Fig. 16. Most of the circuitries and components are hand-made, namely designed and constructed by laboratory staffs and students from fall of 1970 through summer of 1971.

(4) *Detector*

The BF_3 detector 12EB40, manufactured by 20th Century Electronics Ltd. and described in Sec. Ⅳ—2, was used. Additional specification data needed in this section for perturbation calculation are the following: the thickness of copper container is 0.65 mm, the length of the copper container 24.3 cm. In the diffusion length measurement of Sec. Ⅳ, hollow space was left around that part of detector cable which was inside the graphite stack as shown in Fig. 3. To avoid this perturbation, necklace type graphite plugs were placed around the cable for the present experiment.

(5) *Counting System*

Multi-channel Pulse-height Analyzer AN-400 of FUJITSU was used in time-analyzer mode utilizing Multi-scaler Module 03T412X. Its deadtime after registering a pulse in any channel is 22 micro seconds, while waiting time in channel advancing action is 32 micro seconds.

Ⅶ—2. *Measurements*

Measurements were carried out from July 12 through July 23, 1971, on the sixteen stacks listed in Table Ⅳ. An example of decay curve is shown in Fig. 17, which is the one for the stack B_6. The specific parameter setting for this measurement was

Date	:	July 22, 1971
Stack I. D. Number	:	B_6
Beam Current (peak)	:	160 micro amp.

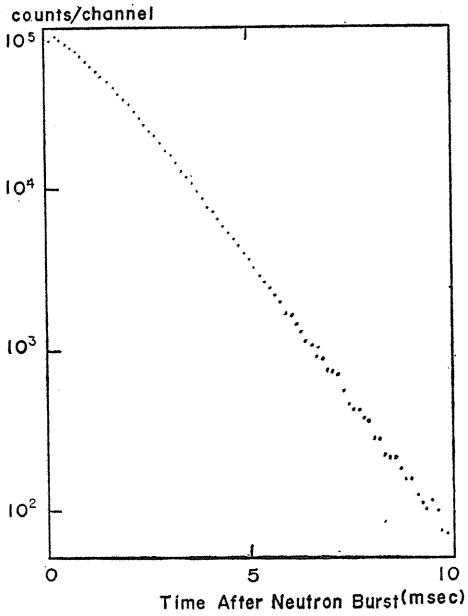

Fig. 17. Pulse-decay Curve for the Stack B_6.

Taable Ⅵ. Measured Decay-Constants and Perturbation Corrections

Stack Identification	λ_{fit} (sec^{-1})	(*1) Perturbation Correction $\Delta\lambda_D$ (sec^{-1})	(*2) λ_{net} (sec^{-1})
B_1	294.54	2.32	292.22
B_2	326.30	3.08	323.22
B_3	431.24	4.56	426.68
B_4	529.26	6.76	522.50
B_5	617.25	10.03	607.22
B_6	793.99	14.11	779.88
B_7	909.32	16.33	892.99
B_8	1090.0	19.38	1070.6
B_9	1244.1	27.28	1216.8
B_{10}	1350.0	31.57	1318.4
B_{11}	1533.2	37.46	1495.7
B_{12}	1561.8	41.46	1520.3
B_{13}	1636.3	46.42	1589.9
B_{14}	1720.1	52.73	1667.4
B_{15}	1809.5	61.02	1748.5
B_{16}	1984.0	72.41	1911.6

(*1) $\Delta\lambda_D$ is given by Eqs. (Ⅶ—2) and (Ⅶ—3).
(*2) $\lambda_{net}=\lambda_{fit}-\Delta\lambda_D$

Pulse Width	: 400 micro sec.
Pulse Frequency	: 25 cps
Duration of Measurement	: 30 min.
Channel Advance	: 128 micro sec.

Least square fitting to the form (const)$\cdot\exp(-\lambda t)$ was programmed and run on FACOM 230/60 at Nagoya University Computation Center. The values of λ determined are tabulated in Table Ⅵ as λ_{fit}. The correction $\Delta\lambda_D$ in this table will be described below.

Ⅶ—3. *Detector Perturbation*

Decay of a pulse within a system is enhanced by insertion of a detector which also absorbs neutrons. To include this additional absorption, we put

$$\lambda_{fit}=\lambda_{net}+\Delta\lambda_D, \qquad (\text{Ⅶ}-1)$$

where λ_{net} indicates the net decay due to leakage from, and absorption within the graphite stack. The amount of perturbation $\Delta\lambda_D$ is given by[51]

$$\Delta\lambda_D=\bar{v}V_D\bar{\Sigma}_D\phi_T^2(\underline{x}_D)/\int_{\text{stack}}\phi_T^2(\underline{x})dV, \qquad (\text{Ⅶ}-2)$$

where V_D is the detector volume about a point $\underline{x}_D$, and Σ_D is the macroscopic absorption cross section of the detector material averaged over thermal energy as in Eq. (Ⅲ—4). The constant $\bar{v}$ is density-averaged thermal neutron speed, which is defined by (Ⅵ—6).

The calculation procedure of $\Delta\lambda_D$ is as follows: As perturbing materials, we consider ^{10}B and copper. The amount of ^{10}B can be evaluated from speifications in Secs. Ⅳ—2 and Ⅵ—3. For copper, it is considered as a hollow cylinder of 2.5 cm diameter, 24.3 cm length and 0.05 cm thickness, and this amount of absorber is smeared over the same volume as that of BF_3 gas, namely a cylinder of 2.5 cm diameter and 12 cm length. The cosine distribution in x, y and z directions is assumed, and the detector position $\underline{x}_D$ is set equal to (0, 0, 0), as it was in the measurement. After the substitution of parameter values, Eq. (Ⅶ—2) gives

$$\Delta\lambda_D=1.115\times10^7\cdot(abc)^{-1}\ (\text{sec}^{-1}). \qquad (\text{Ⅶ}-3)$$

This is the values tabulated in Table Ⅵ as $\Delta\lambda_D$'s.

As described in Sec. Ⅵ—1, a curve of λ_{net} vs. B_0^2 was drawn as illustrated in Fig. 18. Least-square fitting to a quadratic polynomial was made to determine $\bar{v}\bar{\Sigma}_a$, D_0 and C of Eq. (Ⅵ—7). The results are given in Table Ⅶ, together with those by other authors. The constants obtained by the present experiment were corrected for density according to

$$(\bar{v}\bar{\Sigma}_a)_{1.60}=(\bar{v}\bar{\Sigma}_a)_{1.76}\times\left(\frac{1.60}{1.76}\right), \qquad (\text{Ⅶ}-4)$$

$$(D_0)_{1.60}=(D_0)_{1.76}\times\left(\frac{1.76}{1.60}\right), \qquad (\text{Ⅶ}-5)$$

$$(C)_{1.60}=(C)_{1.76}\times\left(\frac{1.76}{1.60}\right)^3, \qquad (\text{Ⅶ}-6)$$

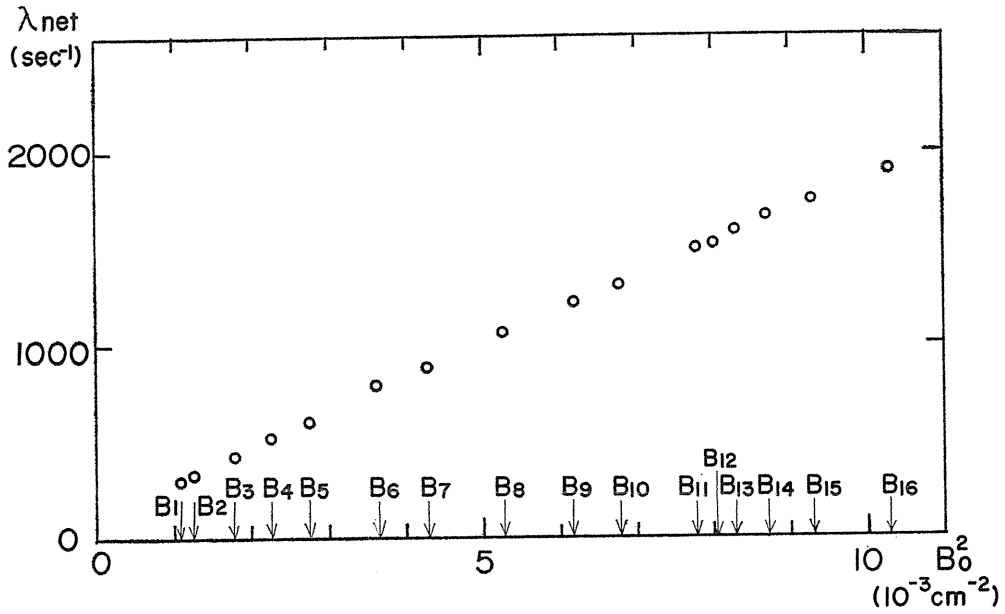

Fig. 18. λ vs. B_0^2 Curve in Pulsed-Neutron Experiment with Graphite (ρ=1.76 gm/cm^3)

Table Ⅶ. Diffusion and Thermalization Parameters by Pulsed-Neutron Method

Author	$\bar{\nu}\bar{\Sigma}_a$ (sec^{-1})	D_0 ($\times 10^5$ cm^2/sec^{-1})	C ($\times 10^5$ cm^4/sec^{-1})	Range of B^2 studied ($\times 10^{-3}cm^{-2}$)	ρ (g/cm^3)
Antonov (Ref. 75)		2.07 ±0.03	1.25±2.0	1.0 ~ 4.0	1.67±2.5%
Beckurts (Ref. 76)		2.13 ±0.02	16.3 ±2.5	0.7 ~ 5.5	1.67±2.5%
Starr and Price (Ref. 77)	75.0 ±0.6	2.14 ±0.01	39 ±3	1.76~18.9	1.60
Honeck (Ref. 78)	60.1	2.178	24.57		
Reed, *et al* (Ref. 79)	81.6 ±1.2	2.145±0.004	21.8 ±1.9	0.930~13.44	1.60
Davis, *et al* (Ref. 80)	73.50±0.06	2.207±0.009	44.2 ±4.1	1.946~12.30	1.60
Sagot and Tallier (Ref. 81)	74 ±3	2.19 ±0.03	39 ±4	0.713~15.49	1.60
Takahashi and Sumita (Ref. 83)	72 ±7	2.27 ±0.04	38.5 ±3.5	1.075~10.41	1.6
Mitsui and Sugiyama (Ref. 82)	93.5 ±5.0	2.01 ±0.03	21.9 ±2.6	2.26 ~15.58	1.60
Present Values (Normalized to ρ=1.60)	76.9 ±2.5	2.15 ±0.02	24.1 ±2.6	1.08 ~10.33	1.60
Present Values	84.6 ±2.7	1.96 ±0.02	18.1 ±1.9	1.08 ~10.33	1.76

where the subscripts 1.60 and 1.76 stand for the quantities at respective densities.

Ⅶ—4. *Discussions*

The present $\bar{v}\bar{\Sigma}_a$ value is 24 % higher than theoretical value by Honeck. Experimental values by other authors also show a tendency to exceed Honeck's value by large amount. This may be an indication that it is difficult in general to obtain pure graphite. Even a very little quantity of impurity, such as boron, could alter $\bar{v}\bar{\Sigma}_a$ value greatly, because of very small absorption cross section of graphite. On the other hand, the value of D_0 can not be influenced much, because there is much less difference in scattering cross sections of various isotopes than in absorption cross sections. Thus D_0 would be determined by the characteristic of graphite itself. Less discrepancies of D_0 values among the authors of Table Ⅶ support this speculation.

Let us look at our values from the view point of consistency with the diffusion length measurement of Sec. Ⅳ. If we calculate diffusion length from $\bar{v}\bar{\Sigma}_a$ and D_0 of Table Ⅶ, it gives

$$L_{1.60}=\sqrt{\frac{D_0}{\bar{v}\bar{\Sigma}_a}}=52.9\pm1.1 \text{ cm}, \qquad (\text{Ⅶ}—7)$$

which is a little larger value than that obtained in Sec. Ⅳ—4. But because the difference is small we conclude that these two sets of values are consistent within experimental error, and that $\bar{v}\bar{\Sigma}_a$ and D_0 in Table Ⅶ must be accurate for this specific batch of graphite.

If this is the case, we suspect that there is much more impurity than was reported by Ref. (31), probably to the extent speculated in Table Ⅲ. Or there may have been contamination of graphite by ambient boron or cadmium, which are the materials frequently used in neutron physics laboratory.

As to the value of C, there has been considerable discrepancies among published values. It has even been suspected[52] that M_2^* value given by (Ⅵ—11) depends on the history of fabrication process for individual batch. Furthermore, the curve fitting procedure can easily result in large error unless there are enough data points on λ-B_0^2 plot with good accuracy. Despite this situation the present C value appears to be in reasonable agreement with others. This again may be the reflection of the fact that good agreements in C and D_0 were possible because they are the quantities related to scattering, whereas for $\bar{v}\bar{\Sigma}_a$ the agreement with others is poor, because of impurities which considerably influence the amount of absorption.

To further refine the present data acquisition and interpretation, the following points have to be improved or corrected for: (a) deadtime in multichannel time analyzer, and (b) absorption by detector cable and connectors which was not included in the perturbation calculation. These factors may cause a different value of L for the pulse experiment from that in diffusion length experiment. The room return neutrons would affect much less in this case than in Sec. Ⅳ, because the graphite stack is coverd by cadmium. The void effect of detector hole has been much diminished, by virtue of the necklace type of graphite plugs around the detector cable, which filled the void.

Ⅷ. Theoretical Complexity of Energy-Dependent Treatment

Theoretical prediction and measurements on pulse decay, as those introduced in Secs. Ⅵ and Ⅶ, had appeared in satisfactory agreement, before more rigorous treatment were attempted. When energy-dependence was introduced into the treatments, people noticed a contradiction. Theories predicted an upper bound for the values of the decay constant λ, whereas experiments exceeded this bound in case of crystalline moderators.[53],[54],[4] Corngold and Durgun[4] solved this problem by introducing a concept of peaked continuum, from which results a so-called pseudo discrete mode. In the following we illustrate their idea with a very simple scattering kernel. Although the model may be unrealistically simple, the model is hoped to elucidate the crux of a relation between theory and experiment.

We start with energy-dependent diffusion equation[49]

$$\frac{1}{v}\frac{\partial\phi(\underline{x},\ v,\ t)}{\partial t}+\mathrm{div}\underline{J}+\Sigma_t(v)\phi$$

$$=\int_0^\infty dv'\Sigma_s(v'\to v)\phi(\underline{x},\ v',\ t)+S(\underline{x})\delta(t)\delta(v-v_0), \qquad (\text{Ⅷ}-1)$$

where $\Sigma_t(v)=\Sigma_a(v)+\Sigma_s(v)$ is the energy-dependent total cross section, $\Sigma_a(v)$ and $\Sigma_s(v)$ are absorption and scattering cross section, respectively. It is assumed that source neutrons are introduced at the upper limit $v_0=v(E_0)$ of thermal energy. Although the upper limit of integration is indicated as ∞, in reality the essential distribution of speed is bounded by this v_0. The speed-, time-, and position-dependent flux $\phi(\underline{x},v,t)$ is assumed to be separated as

$$\phi(\underline{x},\ v,\ t)=\varphi_0(\underline{x})\Psi(v,\ t), \qquad (\text{Ⅷ}-2)$$

where the spatial distribution $\varphi_0(\underline{x})$ is the fundamental mode of the eigenvalue problem

$$\nabla^2\varphi(\underline{x})+B^2\varphi(\underline{x})=0, \qquad (\text{Ⅷ}-3)$$

with eigenvalue B_0^2. The vector $\underline{x}$ denotes a three-dimensional position vector. We also assume that the source has this spatial distribution, namely

$$S(\underline{x})=S_0\varphi_0(\underline{x}). \qquad (\text{Ⅷ}-4)$$

Furthermore, for the scattering kernel $\Sigma_s(v'\to v)$ we employ a separable kernel model[43]

$$\Sigma_s(v'\to v)=A\Sigma_s(v')v\cdot\Sigma_s(v)M(v), \qquad (\text{Ⅷ}-5)$$

which statisfies a requirement of detailed balance relation

$$M(v')v'\Sigma_s(v'\to v)=M(v)v\Sigma_s(v\to v'). \qquad (\text{Ⅷ}-6)$$

Here $M(v)$ is the Maxwellian density distribution

$$M(v)dv=\frac{4}{\sqrt{\pi}}\exp\{-(v/v_T)^2\}\cdot(v^2/v_T^3)dv, \qquad (\text{Ⅷ}-7)$$

where

$$mv_T^2/2=kT.$$

In order that the kernel in Eq. (Ⅷ—5) satisfies the conservation relation

$$\int_0^\infty \sum_s(v'\to v)\,dv=\sum_s(v'), \tag{Ⅷ—8}$$

the constant A has to be taken as

$$A=\left[\int_0^\infty v\sum_s(v)M(v)\,dv\right]^{-1}. \tag{Ⅷ—9}$$

After the substitution of this simple model to Eq. (Ⅷ—1), we take the Laplace transform of the resulting equation, and arrive at the relation

$$\tilde{\Psi}(v,\ s)=\frac{AR_s(v)M(v)}{(s/v)+(DB_0^2+\sum_t)}\int_0^\infty dv'\sum_s(v')\tilde{\Psi}(v',\ s)$$

$$+\frac{S_0\delta(v-v_0)}{(s/v)+(DB_0^2+\sum_t)}, \tag{Ⅷ—10}$$

where

$$R_s(v)\equiv\sum_s(v)\,dv, \tag{Ⅷ—11}$$

and where $\tilde{\Psi}(v,s)$ is the Laplace transform of $\Psi(v,t)$. As a routine procedure we multiply both sides with $\sum_s(v)$ and integrate over v. From the result we can obtain the quantity $\int_0^\infty dv\sum_s(v)\tilde{\Psi}(v,s)$. Substituting the result to Eq. (Ⅷ—10), we obtain an explicit expression for $\tilde{\Psi}(v,s)$:

$$\tilde{\Psi}(v,\ s)=AS_0vM(v)f(s,\ v)\cdot f(s,\ v_0)\cdot\left[1-A\int_0^\infty f(s,\ v)R_s(v)M(v)\,dv\right]^{-1}$$

$$+\frac{S_0f(s,v)\delta(v-v_0)}{\sum_s(v_0)}, \tag{Ⅷ—12}$$

$$f(s,\ v)\equiv\frac{R_s(v)}{s+v\{D(v)B_0^2+\sum_t(v)\}}. \tag{Ⅷ—13}$$

Before we scrutinize the singularities of $\tilde{\Psi}(v,s)$ we place more simplifying assumptions. First we assume that there is no absorption in the medium, and put $\sum_a(v)=0$. Thus the decay of the pulse is only due to leakage. Second, the form of $\sum_s(v)$ is assumed to be

$$\sum_s(v)=\lambda_i/v, \tag{Ⅷ—14}$$

where λ_i is a constant.

Because the detector response is the quantity under investigation in experiments in general, we investigate the behavior of

$$T_D(t)\equiv\int_0^\infty\sum_D(v)\Psi(v,\ t)\,dv, \tag{Ⅷ—15}$$

where $\sum_D(v)$ is the cross section of detector material. For $\sum_D(v)$, we assume a

dependence

$$\Sigma_D(v)=\lambda_D/v, \tag{Ⅷ—16}$$

where λ_D is another constant. Then the Laplace transform $\tilde{T}_D(s)$ of $T_D(t)$ is obtained as

$$\tilde{T}_D(s)=S_0\lambda_D f(s,v_0)F(s)/G(s)+S_0\lambda_D[s+(v_0^2\theta/\lambda_i)+\lambda_i]^{-1} \tag{Ⅷ—17}$$

where

$$\left.\begin{aligned} F(s)&\equiv\int_0^\infty M(v)f(s,\ v)\,dv \\ G(s)&\equiv A^{-1}-\lambda_i\int_0^\infty f(s,\ v)M(v)\,dv \end{aligned}\right\}, \tag{Ⅷ—18}$$

$$\theta\equiv B_0^2/3,$$

and where we have used the usual assumption

$$D=(3\Sigma_s)^{-1}. \tag{Ⅷ—19}$$

There are three kinds of singularities for $\tilde{T}_D(s)$, which are illustrated in Fig. 19. They are:

(a) Pole at

$$s=-p_F=-\left[\frac{\theta}{\lambda_i}v_0^2+\lambda_i\right]. \tag{Ⅷ—20}$$

Because v_0 is the maximum of speed v involved, this pole is at the far end of the cut described in (c) below. This pole corresponds to the physical fact that the source neutrons have the speed v_0.

(b) The discrete root s_D which satisfies the dispersion relation

$$G(s_D)=0. \tag{Ⅷ—21}$$

This pole reflects thermalization process, and it gives rise to the mode determined in Secs. Ⅵ and Ⅶ. To see this connection, replace $M(v)$ in the expression of $G(s)$ by $\delta(v-\bar{v})$, then we obtain an analogous relation to (Ⅵ—5) with no absorption.

(c) The cut given by

$$s=-\left[\frac{\theta}{\lambda_i}v_c^2+\lambda_i\right],\quad 0\leq v_c\leq\infty. \tag{Ⅷ—22}$$

Any s given by (Ⅷ—22) makes the denominator in the integrand of $\int_0^\infty f(s,\ v)\,M(v)\,dv$ in $G(s)$ vanish at a point $v=v_c$. Across this cut, there is a jump of values for both $F(s)$ and $G(s)$, which will be given in the following.

Noting these singularities we invert $\tilde{T}_D(s)$ of (Ⅷ—17). We write the inversion of the first term as a contour integral along I_1 (Fig. 19), while the inversion of the second term will be denoted by $T_{DS2}(t)$; namely

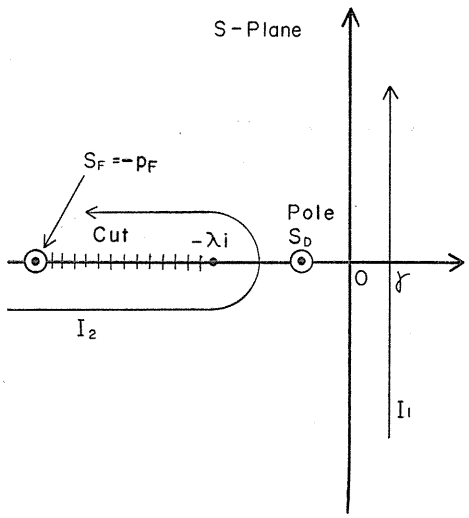

Fig. 19. Singularities of $\tilde{T}_D(s)$, and Contour of Integration. The Cut is Given by Eq. (Ⅷ—22).

$$T_D(t)=\frac{1}{2\pi i}\int_{\gamma-i\infty}^{\gamma+i\infty}\frac{S_0\lambda_D f(s,v_0)F(s)}{G(s)}e^{st}dt+T_{DS2}(t). \qquad (Ⅷ—23)$$

The term $T_{DS2}(t)$ is immediately obtained as

$$T_{DS2}(t)=S_0\lambda_D\exp(-p_F t), \qquad (Ⅷ—24)$$

which is the residue at $s=-p_F$. The first term of Eq. (Ⅷ—23) can be separated into three parts;

(1) The residue at the pole s_D:

$$T_{DD}(t)=S_0\lambda_D f(s_D,v_0)F(s_D)\exp(s_D t)/G'(s_D). \qquad (Ⅷ—25)$$

(2) The integral along the contour I_2 in Fig. 19:

$$T_{DC}(t)=\frac{1}{2\pi i}\int_{\lambda_i}^{\infty}S_0\lambda_D f(-p,\ v_0)e^{-pt}\left\{\frac{F^-(-p)}{G^-(-p)}-\frac{F^+(-p)}{G^+(-p)}\right\}dp. \qquad (Ⅷ—26)$$

(3) The residue at $s=-p_F$. For a general case where this pole is imbedded in the cut, it has to be evaluated by integrals above and below the cut:

$$T_{DS1}(t)=\frac{1}{2}S_0\lambda_D R_S(v_0)\,e^{-p_F t}\left\{\frac{F^-(-p_F)}{G^-(-p_F)}+\frac{F^+(-p_F)}{G^+(-p_F)}\right\}. \qquad (Ⅷ—27)$$

The notations in the above equations will be explained in the course of following discussions. To summarize the above definitions, the detector response is given as

$$T_D(t)=T_{DD}(t)+T_{DC}(t)+T_{DS1}(t)+T_{DS2}(t). \qquad (Ⅷ—28)$$

In Eq. (Ⅷ—28), $T_{DS1}(t)$ and $T_{DS2}(t)$ give the decay of neutrons with source speed. The former is due to the neutrons who keep the original speed v_0 even after collisions.[55],[56] Functional forms of $F^{\pm}(-p)$, $G^{\pm}(-p)$ will be given later. The term $T_{DS2}(t)$ is the direct contribution from the source itself, which is distributed

over the system in fundamental spatial mode. In actual experiments, $T_{DS1}(t)$ and $T_{DS2}(t)$ decay faster than other terms in (Ⅷ—28). Furthermore, they have little significance in studying thermalization phenomena. Therefore in the following we concentrate our effort on $T_{DD}(t)$ and $T_{DC}(t)$.

The term $T_{DD}(t)$, which we call discrete mode, is the main subject of pulsed-neutron experiment. The experiment of the type in Sec. Ⅵ is based on the assumption that there exists a root s_D, and that if one waits long enough after the pulse, this mode dominates over others. If a pole s_D ever exists on the s-plane of Fig. 19, this indeed would be the case, because other singularities are to the left of s_D.

To be more precise, by examining the dispersion relation (Ⅷ—21) the following natures of s_D can be concluded.

(1) s_D is real and negative.
(2) The dispersion relation (Ⅷ—21) has one discrete root at most.
(3) For $B_0^2=0$ (which means infinite medium), s_D becomes zero, which is to be expected for medium without absorption.
(4) As B_0^2 increases, s_D decreases. In other words the root moves toward the branch point $s=-\lambda_i$.

The term $T_{DC}(t)$, which often is called continuum, originates from the jump of values in $F(s)$ and $G(s)$ across the cut. Since s can be put as

$$s=-p\pm i\varepsilon, \quad \lambda_i<p<\infty \tag{Ⅷ—29}$$

above and below the cut, we need to know the following functions:

$$F^{\pm}(-p)\equiv F(-p\pm i\varepsilon)=\lambda_i\int_0^{\infty}\frac{M(v)dv}{\lambda_i+\theta v^2/\lambda_i-p\pm i\varepsilon}, \tag{Ⅷ—30}$$

$$G^{\pm}(-p)\equiv G(-p\pm i\varepsilon)=\frac{1}{A}-\lambda_i^2\int_0^{\infty}\frac{M(v)dv}{\lambda_i+\theta v^2/\lambda_i-p\pm i\varepsilon}, \tag{Ⅷ—31}$$

with ε tending to zero. The denominators of these integrals become zero at the speed

$$v_\lambda(p)\equiv\sqrt{\lambda_i(p-\lambda_i)/\theta}, \tag{Ⅷ—32}$$

if $\varepsilon=0$. For this kind of integral we can employ a formula[57],[58]

$$\lim_{\varepsilon\to+0}\frac{1}{x-x_0\pm i\varepsilon}=P\frac{1}{x-x_0}\mp i\pi\delta(x-x_0), \tag{Ⅷ—33}$$

which applies to an integral over a region including x_0. Here P indicates Cauchy's principal value integral, and $\delta(x-x_0)$ is Dirac's delta function. In our case, the following more general formula is suitable:

$$\lim_{\varepsilon\to+0}\frac{1}{y(x)\pm i\varepsilon}=P\frac{1}{y(x)}\mp i\pi\frac{i\pi\delta(x-x_0)}{|y'(x_0)|}, \tag{Ⅷ—34}$$

for a single-valued, monotonic function $y(x)$ with a relation $y(x_0)=0$. Then $F^{\pm}(-p)$, and $G^{\pm}(-p)$ can be written as follows:

$$\left.\begin{aligned} F(-p\pm i\varepsilon) &= F_0(p)\mp iF_1(p) \\ G(-p\pm i\varepsilon) &= G_0(p)\mp iG_1(p), \end{aligned}\right\} \qquad (\text{Ⅷ}-35)$$

where

$$F_0(p)\equiv\lambda_i P\int_0^\infty \frac{M(v)dv}{(\theta/\lambda_i)v^2-(p-\lambda_i)}, \qquad (\text{Ⅷ}-36)$$

$$F_1(p)\equiv\pi\lambda_i\frac{\lambda_i M[v_\lambda(p)]}{2\theta v_\lambda(p)}, \qquad (\text{Ⅷ}-37)$$

$$G_0(p)\equiv\lambda_i\left\{1-\lambda_i P\int_0^\infty \frac{M(v)dv}{(\theta/\lambda_i)v^2-(p-\lambda_i)}\right\}, \qquad (\text{Ⅷ}-38)$$

$$G_1(p)\equiv-\pi\lambda_i^2\frac{\lambda_i M[v_\lambda(p)]}{2\theta v_\lambda(p)}. \qquad (\text{Ⅷ}-39)$$

Note that $F_1(\lambda_i)=G_1(\lambda_i)=0$. Note also that these functions are defined for those values of p which are on the cut. Therefore in Eqs. (Ⅷ—36) through (Ⅷ—39), it is understood that $p\geqslant\lambda_i$.

Now we consider the relation of the discrete mode $T_{DD}(t)$ with experiment. As stated above, the pole s_D moves along the negative real axis toward the branch point $-\lambda_i$, as the system size gets smaller, and as B_0^2 increases. Then there should be a certain value of B_0^2, say B_0^{*2}, for which s_D coincides with $s=-\lambda_i$. Beyond this limit, there can be no single exponential decay, but we would observe the decay of the continuum $T_{DC}(t)$. Then from an experiment beyond this B_0^{*2} one would be unable to extract any physical parameters. Then why did experimentalists reported measuring s smaller than $-\lambda_i$?

We recall that such a paradox was reported for crystalline moderators, which have discontinuity of scattering cross section at Bragg cut-off speed v_B. Such a discontinuity is not included in our model, and therefore we cannot illustrate here the precise behavior of $T_{DC}(t)$ for crystalline moderator. The discontinuity is essential for the interpretation of the paradox. The following illustration with continuous cross section model, however, will help readers derive an analogous picture for the discontinous cross section.

For this purpose we examine the behavior of the integrand in $T_{DC}(t)$: we write this integral as

$$T_{DC}(t)=(\pi)^{-1}\int_{\lambda_i}^\infty S_0\lambda_D f(-p,\ v_0)K(p)\exp(-pt)dp, \qquad (\text{Ⅷ}-40)$$

with

$$K(p)\equiv\frac{1}{2i}\left\{\frac{F^-(-p)}{G^-(-p)}-\frac{F^+(-p)}{G^+(-p)}\right\}=\frac{F_1G_0-F_0G_1}{G_0^2+G_1^2}. \qquad (\text{Ⅷ}-41)$$

The principal value integrals of F_0 and G_0 in (Ⅷ—36) and (Ⅷ—38) are in the following form:

$$P\int_0^\infty\frac{x^2\exp(-x^2)}{x^2-k^2}dx=\int_0^\infty e^{-x^2}dx+\frac{k}{2}P\int_{-\infty}^\infty\exp(-x^2)dx/(x-k),$$

where k is a constant. For the second term we can make use of a general formula[59]

$$P\int_{-\infty}^{\infty}\exp(-x^2)dx/(x-k)=-2\sqrt{\pi}\,e^{-k^2}\int_0^k e^{t^2}dt. \qquad (\text{VIII}-42)$$

After rearrangement with the help of this formula, $K(p)$ can be written as follows:

$$K(p)=K_1(p)/\{K_2^2(p)+K_3^2(p)\} \qquad (\text{VIII}-43)$$

where

$$K_1(p)=2\sqrt{\pi}\zeta\rho\exp(-\rho^2),$$

$$K_2(p)=1-2\lambda_i\zeta\{1-2\rho\exp(-\rho^2)\int_0^\rho e^{t^2}dt\},$$

$$K_3(p)=2\sqrt{\pi}\lambda_i\zeta\rho\exp(-\rho^2),$$

where

$$\rho=\rho(p)=v_\lambda(p)/v_T,\quad \zeta=\lambda_i/(\theta v_T^2).$$

From Eq. (VIII—43) we see that the amplitude $K(p)$ of the continuum $T_{DC}(t)$ has a maximum for a value of ρ whose magnitude is of the order of unity. Suppose this value of ρ, which we call ρ_0, corresponds to $p=p_0$. As a consequence of the peak, the decay of $\exp(-p_0t)$ will be dominant over all other $\exp(-pt)$ components with p distributed over $(-\infty, -\lambda_i)$.

According to Corngold and Durgun, however, numerical calculations showed that the peak of $K(p)$ for continuous $\Sigma_s(v)$ is not so pronounced. For cystalline moderators, on the other hand, there is a jump of $\Sigma_s(v)$ value, and this gives rise to a very sharp peak of $K(p)$ for B_0^2 exceeding B_0^{*2}. Such a peak occurs at the root of

$$G_0(p_0)=0. \qquad (\text{VIII}-44)$$

For this case, then, $K(p)$ can be approximated by

$$K(p)\approx\frac{-F_0(p_0)G_1(p_0)}{\{G_0'(p_0)\}^2(p-p_0)^2+G_1^2(p_0)} \qquad (\text{VIII}-45)$$

which is derived by Taylor expansion of $G_0(p)$ in the denominator about p_0. From (VIII—45) we see that near the peak, $K(p)$ has a distribution of Breit-Wigner type, and its full width at half-maximum is equal to

$$\Gamma=2|G_1(p_0)/G_0'(p_0)|. \qquad (\text{VIII}-46)$$

Furthermore, it turns out that $G_1(p_0)$ for crystalline moderator is proportional to the distance between negative real axis and the pole s_D on the adjacent Riemann sheet, which are found by analytic continuation of the dispersion relation (VIII—21) beyond the cut.

Thus when the distance of the poles and negative real axis is short, the peak of $K(p)$ at p_0 is quite pronounced. For experimentalists the continuum $T_{DC}(t)$ then appears in effect as a single exponential decay. This decay pattern was named

"pseudo discrete mode."

We have sketched the model developed by Corngold and Durgun. Its limitation is that it is based on diffusion equation, and on the separable kernel (Ⅷ—5). When these points are improved,[55],[56] the prediction surely becomes more precise, but the picture becomes too complicated, and its essential point is obscured. We have attempted therefore to illustrate their idea as clear as possible with a simple model.

Ⅸ. Investigations That Followed and Possibility for Further Studies

After the two series of experiments which we have reported, other experiments were carried out in the following several years with this graphite. Among the subjects of investigations are:

(1) determination of slowing-down time,
(2) perturbation by strong absorbers on pulse-decay constant,
(3) measurement of angle-dependent neutron current in graphite,
(4) neutron wave propagation experiment in graphite,
(5) neutron wave propagation in a two-region (graphite-iron) system,
(6) effect of cadmium shutter placed between thermalization layer and graphite stack,
(7) leakage fast neutron spectrum from graphite slab.

The study (4) was carried out with a novel method of data analysis and circuitry,[60] and led to a discovery of wave interference pattern between epithermal neutrons and thermal neutrons.[61] This interference had not been expected for this simple arrangement of a graphite stack and a neutron generator. It is in contrast to the interference between cold neutrons and thermal neutrons:[62],[63],[64] thus it appears that whenever there are two energy groups of neutrons whose propagation laws are markedly different one can find such an interference. Because of the similarity between the two patterns of interference, much analogy could be drawn from the study[65],[66] on the interference observed by Utsuro *et al*,[62] and Takahashi.[63] The concept gained in neutron wave experiments with graphite could be utilized later in understanding dynamical behavior of multiplying medium.[67]

The graphite is now being used as standard material in fast neutron spectroscopy. The latter study is in progress to study neutron transport in fusion reactor blanket material such as lithium.

In the following we will briefly explore the possibility for future investigations on neutron transport within moderators in general.

(1) Pulse-decay experiment for a two-region system: The decay described by Eq. (Ⅵ—4) can be written as

$$\phi_T(x,t)\sim\exp(t/\Lambda)$$

where Λ is neutron lifetime. Therefore, by pulsed-neutron experiment with a two region system one can determine Λ for the system. This will give one a clue for understanding the law of interaction between the two regions from the viewpoint of neutron life.

(2) Graphite as standard material: With the accumulation of accurate data on graphite one can determine the perturbation caused by small sample, from which one can infer the reactor physics parameter of the sample both in fast and thermal

energy regions. A shift in neutron-wave interference pattern, for example, could be utilized in this connection.

(3) Discontinuity of λ-B_0^2 curve: For polycrystals λ-B_0^2 curve has a discontinuity[55] near λ^*, which is the value of λ corresponding to B_0^{*2}. For graphite, this discontinuity is too small to be detected. For other polycrystals, however, there may be a large enough discontinuity. It is meaningful to investigate how this gap can be determined, and how the finding can be utilized.

(4) Systematic study of neutron flux around the target of neutron generator: In this country many accelerators are under costruction, or being designed as intense neutron sources. There is very few systematic studies, however[68], in obtaining desired neutron flux of specified energy spectrum and spatial distributions. Such studies would not only save labor and machine time in these installations, but also would have much application in accelerator breeding and incineration.[69] The feasibility of the latter is now being studied seriously in the world in connection with nuclear fuel cycles.

(5) Differential informations from integral experiments: So far our report has been limited to integral experiments, in the sense that we have detected neutrons regardless what energy they have. Thus the detector counts represented neutron absorption per second integrated over energy.

But most of the informations needed nowadays in neutron physics or reactor physics are differential data, such as energy dependent scattering cross section $\sum_s(E)$, or scattering kernel $\sum_s(E\to E')$. This can be said both in fast (MeV range) and thermal regions of energy. Then a question arises: how can one extract differential informations effectively out of integral experiments?

One solution is to make as much use of integral experiments as possible in a meticulous manner. Interference observation in wave experiment is one example. Although the observation is made by integrated quanity, this phenomenon provided a rough estimate of energy spectrum in cold-plus-thermal neutron experiment, or fast-plus-thermal neutron experiment. If one wants more detailed differential data, the most natural solution would be to modify the experiments to a differential type, namely to observe energy spectrum. Then much more about scattering kernel can be inferred. Kawakita and Takahashi[70] made such an attempt in analyzing their data on cold-to-thermal energy spectrum in graphite.

While these attempts in thermal range are rather academic, the differential data in 14 MeV range in general would almost have an immediate influence on the engineering study of fusion reactor blanket. For this reason, much effort is being made over the country and overseas to gain informations on energy dependent cross section of various neutron-induced reactions in this energy region. Lithium is the material attracting much attention, and attempts have been made to infer its inelastic scattering cross sections with various level of nucleus excitation.[71]

In this connection, the graphite in our laboratory is being used as a standard test material for various techniques in fast neutron spectroscopy.[72] Determination of leakage fast neutron spectra from lithium assemblies are being carried out at the same time, and comparison with the results of Monte Carlo calculation or transport calculations is made.[73],[74] From this comparison, flaws in nuclear data can be inferred.

So far these attempts in fast neutron spectroscopy seem to have been quite successful, and there is much room for more effort that will be rewarding. One reason is that the nuclear data in this energy range have been meager compared

with lower ranges of energy. Thus what can be inferred from energy spectrum, which still is a kind of integral data, have been valuable. When the incompleteness in nuclear data is improved, can one still point out detailed flaws from integral exteriment? Can we compete with differential data obtained directly from cross section measurement? Then one would face a similar situation in fast energy range as he does now in thermal range. In fast energy range, neutrons which have experienced only few number of collisions with the medium nuclei determine the spectrum, and this makes his prediction of differential data by Monte Carlo analysis easy. At the same time, this fact inevitably accompanies strong anisotropy in the angular distribution of neutron flux, and special measure is needed in solving transport equation.[71]

In thermal range, functional forms of scattering kernels have been well-known, and what he has to infer is probably several adjustable parameters. It is easier for him to examine the validity of differential data in this sense. But the spectrum is determined by neutrons that have undergone many collisions. This makes extraction of differntial data more difficult.

X. Acknowledgement

We express our gratitude to Prof. K. Sumita of Osaka University, and Dr. Y. Kaneko of Japan Atomic Energy Research Institute, who gave valuable suggestions and made helpful arrangements on the graphite experiments reported here.

This series of experiments were planned, designed and carried out in eighteen months since the delivery of graphite. Such schedule was made possible only by collaboration of staff members, graduate- and undergraduate students. We reflect upon these experiments with fond memories of these active members. In particular, Messrs. Z. Suzuoki, and S. Mizuno worked on the beam transport system, ion souce, and pulsing electronic circuits with devotion. Messrs. K. Kawano and N. Harao helped us on every aspect of equipment preparations. Theoretical analysis was carried out with the help of Messrs. K. Nunome, K. Kawaguchi, R. Asano and S. Suzuki. Among other people who worked on this experiment then as students are Messrs. O. Kawabata, K. Okamoto, M. Hirano, T. Asami, K. Nakashima, R. Kanda and T. Akutagawa.

Helps offered by A. Inoue, S. Wakamatsu and K. Hashimoto in preparing the figures, tables and numerical values in this review are appreciated.

The numerical calculations needed in the above analysis were carried out with FACOM 230/60 computer at Nagoya University Computation Center.

Efficient typing provided by Miss A. Suzuki for preparation of this manuscript is greatly appreciated.

References

1) I. Kuščer, "Advances in Neutron Thermalization Theory," *Proc. Symp. Neutron Thermalizaiton and Reactor Spectra*, Ann Arbor, Michigan Vol. I, SM-96/103, pp. 3-26, IAEA, Vienna (1967).

2,) N. Corngold, "Quasi-Exponential Decay of Neutron Fields," *Advances in Nuclear*

Science and Technology, E. J. Henley and J. Lewins, Editors, Vol. 8, pp. 1-46, Academic Press, New York (1975).
3) M. M. R. Williams, "Existence of a Diffusion Length in a Finite Prism of Pure Moderator," *Proc. Symp. Neutron Thermalization and Reactor Spectra*, Ann Arbor, Michigan, Vol. I, SM-96/3, pp. 27-43, IAEA, Vienna (1967).
4) N. Corngold and K. Durgun, "Analysis of Pulsed-Neutron Experiments in Moderators via a Simple Model," *Nucl. Sci. Eng.*, **29**, 354-366 (1967).
5) S. Glasstone, and M. C. Edlund, *The Elements of Nuclear Reactor Theory*, Sections 5.61-5.91, D. Van Nostrand Co., New York (1952).
Translated into Japanese by K. Fushimi and M. Ohtsuka, and published by Misuzu-shobo (1955).
6) C. R. Richey and E. Z. Block, "Graphite Diffusion Length Measurements at Hanford," HW-45035, U. S. Atomic Energy Commission Research and Development Report (1956).
7) J. R. Lamarsh, *Introduction to Nuclear Reactor Theory*, Section 5.8, Addison-Wesley Publishing Company, Reading, Massachusetts (1966).
Translated into Japanese by A. Takeda and K. Nishina, and published by Yoshioka-shoten (Vol. I in 1974, Vol. II in 1976).
8) G. von Dardel, "A Study of the Interaction of Neutrons with Moderating Materials," *Phys. Rev.*, **94**, 1272 (1954).
9) G. von Dardel and N. Sjöstrand, "Diffusion Parameters of Thermal Neutrons in Water," *ibid.*, **96**, 1245 (1954).
10) A. M. Weinberg and E. P. Wingner, *The Physical Theory of Neutron Chain Reactors*, pp. 212-213, The University of Chicago Press (1958).
11) A. M. Weinberg and H. C. Schweinler, "Theory of Oscillating Absorber in a Chain Reactor," *Phys. Rev.*, **74**, 851-863 (1948).
12) V. Raievski and J. Horowitz, "Determination of the Mean Transfer Free Path of Thermal Neutrons by Measurement of the Complex Diffusion Length," *Proc. Int. Conf. Peaceful Uses At. Energy*, Vol. 5, P/360, pp. 42-51, Geneva (1955).
13) M. Nelkin, "The Diffusion Cooling of Neutrons in a Finite Moderator," *J. Nucl. Energy*, 8, 48-58 (1958).
14) L. S. Kothari and K. S. Singwi, "Interaction of Thermal Neutrons with Solids," *Solid State Physics*, Vol. 8, pp. 109-190, Academic Press Inc., New York (1959).
15) M. Nelkin, "The Decay of a Thermalized Neutron Pulse," *Nucl. Sci. Eng.*, **7**, 210-216 (1960).
16) *Proceedings of the Brookhaven Conference on Neutron Thermalization*, BNL-719, U. S. Atomic Energy Commission (1962).
17) N. Corngold, "Four Lectures on Neutron Thermalizations," *Lectures from the Second Neutron Physics Conference* (Boyne Mountain, Michigan, 1962), p. 186, Michigan Memorial Phoenix Project (1964).
18) idem., "Some Transient Phenomena in Thermalization," *Nucl. Sci. Eng.*, **19**, 80-90 (1964).
19) N. Corngold, P. Michael, and W. Wollman, "The Time Decay Constants in Neutron Thermalization," *ibid.*, **15**, 13-19 (1963).
20) *"Pulsed Neutron Research," Proc. Symp. Pulsed Neutron Research*, Karlsruhe Vol. I, IAEA, Vienna (1965).
21) *"Neutron Thermalization and Reactor Spectra," Proc. Symp. Neutron Thermalization and Reactor Spectra*, Ann Arbor, Michigan, Vol. I, IAEA, Vienna (1967).
22) Ref. (7), Sections 5.9 and 5.11.
23) Ref. (10), pp. 199-208.
24) Ref. (10), pp. 340-343.
25) K. H. Beckurts and K. Wirtz, *Neutron Physics*, p. 99, Springer-Verlag, New York (1964).
26) O. Kawabata, "Measurement of Graphite Diffusion Length," Graduation Report, Nuclear Engineering Department, Nagoya University (1971, in Japanese).
27) I. N. Sneddon, *Fourier Transforms*, Eq. (69), p. 223, McGraw-Hill, New York (1951).

28) Ref. (10), pp. 325-326.
29) Ref. (7), Problem 5.27.
30) F. A. Valente, *A Manual of Experiments in Reactor Physics*, pp. 194-195, Mcmillan Co., New York (1963).
31) "Test Data on Dimension, Density and Purity Specification of Graphite Blocks for Neutron Experiments," Showa Denko Inc. (March 1970, in Japanese).
32) "Boron Trifluoride and Boron-Lined Neutron Detectors for Nuclear Instrumentation," Catalogue of Twentieth Century Electronics Ltd. (1970).
33) S. F. Mughabghab and D. I. Garber, *Neutron Cross Sections*, Vol, 1, BNL-325, 3rd Ed., p. 5.1, National Neutron Cross Section Center, Brookhaven National Laboratory, New York (1973).
34) Ref. (30), p. 67.
35) J. B. Hoag, *Nuclear Reactor Experiments*, pp. 12-14, D. Van Nostrand Co., New York (1958).
36) W. J. Price, *Nuclear Radiation Detection*, 2nd Ed., Section 10.18, McGraw-Hill, New York (1964).
Translated into Japanese by O. Nishino and A. Sekiguchi and published by Corona-sha (1966).
37) D. A. Daavettila, K. C. Ruzich, W. F. Gilbert, J. Spalek, L. L. Lawyer and W. J. Sturm, "A Manual of Reactor Laboratory Experiments," ANL-6990, p. 27.4, Argonne National Laboratory, U. S. Atomic Energy Commission (1965).
38) M. N. Thompson and J. M. Taylor, "Neutron Spectra from Am-α-Be and Ra-α- Be Sources," *Nucl. Instr. and Method.*, **37**, 305-308 (1965).
39) D. J. Hughes and R. B. Schwartz, *Neutron Cross Section*, BNL-325, 2nd Ed., Brookhaven National Laboratory, U. S. Atomic Energy Commission (1958).
40) L. S. Kothari and V. P. Duggal, "Scattering of Thermal Neutrons from Solids and Their Thermalization near Equilibrium," *Advances in Nuclear Science and Technology*, E. J. Henley, and H. Kouts, Editors, Vol. 2, pp. 186-302, Academic Press, New York (1964).
41) M. Abramowitz and I. A. Stegun, *Handbook of Mathematical Functions*, Formula #7.1.23, Dover, Now York (1965).
42) G. I. Bell and S. Glasstone, *Nuclear Reactor Theory*, Eq. (1.30), Van Nostrand Reinhold Co., New York (1970).
43) M. M. R. Williams, *The Slowing-Down and Thermalization of Neutrons*, p. 15, North-Holland Publishing Co., Amsterdam (1966).
44) Ref. (10) pp. 378-379 and pp. 397-404.
45) J. H. Ferziger and P. R. Zweifel, *The Theory of Neutron Slowing-Down in Nuclear Reactors*, pp. 25-44, pp. 283-287, The M. I. T. Press, Cambridge, Massachusetts (1966).
46) Ref. (30), pp. 103-121.
47) K. Sumita and Y. Kaneko, "Investigation of Slowing-Down and Diffusion with Pulsed-Neutron Method," *Journ. Atomic Energy Soc. Japan*, **3**〔8〕, 634-650 (1961, in Japanese).
48) Ref. (10), pp. 323-324.
49) Ref. (25), pp. 213-216.
50) S. Sawada, "Fabrication of Neutron Monitor with Use of Associated α-Particle Method and Determination of Neutron Yield," Graduation Report, Nuclear Engineering Department, Nagoya University (1978, in Japanese).
51) Ref. (7), Problem 15-6.
52) Y. Kaneko, private communication (1971).
53) J. Wood, "Time and Space Eigenvalue of the Boltzmann Equation," *Proc. Symp. Pulsed Neutron Research*, Karlsruhe, Vol, I, SM-62/44, pp. 219-238, IAEA, Vienna (1965).
54) Ref. (43), p. 170.
55) R. Conn and N. Corngold, "A Theory of Pulsed Neutron Experiments in Polycrystalline Media," *Nucl. Sci. Eng.*, **37**, 85-93 (1969).
56) R. Conn and N. Corngold, "Analysis of Pulsed Neutrn Experiments in Polycrystalline

Media Using a Model Kernel," *ibid.*, **37**, 94–103 (1969).
57) A. Messiah, *Quantum Mechanics*, Vol. I, Eq. (A. 15e), p. 469, North-Holland Publishing Co., Amsterdam (1966).
58) F. D. Gakhov, *Boundary Value Problems*, Pergamon Press, Oxford (1966).
59) B. D. Fried and S. D. Conte, *The Plasma Dispersion Function*, Academic Press, New York (1961).
60) Y. Yamane annd H. Tamagawa, "A New Mehtod of Neutron Wave Measurements," *J. Nucl. Sci. Technol.*, **12** [12], 722–774 (1975).
61) Y. Yamane, K. Nishina and H. Tamagawa, "The Neutron Wava Interference Associated with the Neutron Slowing-Down in Graphite," *Atomkernenergie*, **30**, 36–38 (1977).
62) M. Utsuro, K. Inoue and T. Shibata, "Bragg Cut-off Effects on Neutron Wave Propagation in Graphite," *J. Nucl. Sci Technol.*, **5**, 298–308 (1968).
63) A. Takahashi, "Effect of Cold Neutrons on the Neutron Pulse and Wave Propagation in Crystalline Media," *ibid.*, **9**, 172–184 (1972).
64) N. Yamamuro, Y. Kaneko, T. Nakamura, A. Furuhashi, K. Nishina, A. Takahashi and K. Sumita, "Kinetic Measurements in Reactor Physics," *Journ. Atomic Energy Soc. Japan*, **16**, 111–127 (1974, in Japanese).
65) K. Nishina, "Energy-Dependent Diffusion Theory Treatment of Neutron Wave Propagation in a Finite Medium," Ph. D. Thesis, University of Michigan (1968).
66) K. Nishina and A. Z. Akcasu, "Neutron Wave Analysis in Finite Media," *Nucl. Sci. Eng.*, **39**, 170–181 (1970).
67) M. Shinkawa, Y. Yamane, K. Nishina and H. Tamagawa, "Theoretical Analysis of Coupled-Core Reactors with the Method of the Moderator Region Response Function," *Nucl. Sci. Eng.*, **67**, 19–33 (1978).
68) K. Inoue, "Neutronics of Moderator Assembly Around a Target of Neutron Generator," *Reactor Physics Research*, Circular of Reactor Physics Joint Committee [26], 7, Atomic Energy Soc. Japan (1978).
69) M. Steinberg *et. al.*, "Linear Accelerator-Breeder, a Preliminary Analysis and Proposal," BNL-50592, Brookhaven National Laboratoy (1976).
70) T. Kawakita and A. Takahashi, "Measurements of Pseudo-Decay-Constants of Trapped Neutrons in Small Graphite Systems at 77 and 194°K," *J. Nucl. Sci. Technol.*, **13**, 555–565 (1976).
71) A. Takahashi, J. Yamamoto, M. Ebisuya and K. Sumita, "Method for Calculating Anisotropic Neutron Transport Using Scattering Kernel without Polynomial Expansion," *ibid.*, **16**, 1–15 (1979).
72) K. Ogura, "Graphite Penetration Spectrum of Am–Be Source Neutrons," Graduation Report, Nuclear Engineering Department, Nagoya University (1975, in Japanese).
73) S. Itoh, Y. Seki and H. Maekawa, "Measurements and Calculations of Fast Neutron Spectra in a Graphite-Reflected Lithium Assembly," *Proc. 3rd ANS Topical Mtg. Technol. Controlled Nuclear Fusion*, Santa Fe, New Mexico (1978).
74) I. Mitsuhashi, "The Calculation of Leakage Neutron Spectrum from a Metalic Lithium Assembly Using the Monte Carlo Method," Master Thesis, Nuclear Engineering Department, Nagoya University (1979, in Japanese).
75) A. V. Antonov, A. I. Isakoff, I. D. Murin, B. A. Neupocoyev, I. M. Frank, F. S. Shapiro and I. V. Shtranich, "A Study of Neutron Diffusion in Beryllium, Graphite and Water by the Impulse Method," *Proc. Int. Conf. Peaceful Uses At. Energy*, Vol. 5, P/661, pp. 3–12, Geneva (1955).
76) K. Beckurts, "Measurements with a Pulsed Neutron Source," *Nucl. Sci. Eng.*, **2**, 516–522 (1957).
77) E. Starr and G. A. Price, "Measurement of the Diffusion parameters of Graphite and Graphite-Bismuth by Pulsed Neutron Method," BNL-719, Vol. 3, pp. 1034–1073, Brookhaven National Laboratory (1962).
78) H. C. Honeck, "On the Calculation of Thermal Neutron Diffusion Parameters," BNL-719, Vol. 4, pp. 1186–1210, Brookhaven National Laboratory (1962).

79) C. H. Reed, C. N. Henry and A. A. Usner, "Decay of Thermalized Neutron Fields in Graphite," *Nucl. Sci. Eng*, **30**, 362-373 (1967).
80) S. K. Davis, J. A. DeJuren and M. Reier, "Pulsed-Decay and Extrapolation-Length Measurements in Graphite," *Nucl. Sci. Eng.*, **23**, 74-81 (1965).
81) M. Sagot and H. Tellier, "Mesure des paramètres de diffusion du graphite," *J. Nucl. Energy Pt. A/B*, **17**, 347-348 (1963).
82) J. Mitsui and K. Sugiyama, "Neutron Thermalization in Graphite," *J. Nucl. Technol.*, **10**, 1-9 (1972).
83) A. Takahashi and K. Sumita, "Pulse Propagation Experiments of Thermal Neutrons in Graphite," *J. Nucl. Sci. Technol.*, **5**, 7-17 (1968).